

From Few-Shot to Zero-Shot: Towards Generalist Graph Anomaly Detection

Yixin Liu, Shiyuan Li, Yu Zheng, Qingfeng Chen, Chengqi Zhang, *Fellow, IEEE*,
Philip S. Yu, *Life Fellow, IEEE*, Shirui Pan, *Senior Member, IEEE*

Abstract—Graph anomaly detection (GAD) is critical for identifying abnormal nodes in graph-structured data from diverse domains, including cybersecurity and social networks. The existing GAD methods often focus on the learning paradigms of “one-model-for-one-dataset”, requiring dataset-specific training for each dataset to achieve optimal performance. However, this paradigm suffers from significant limitations, such as high computational and data costs, limited generalization and transferability to new datasets, and challenges in privacy-sensitive scenarios where access to full datasets or sufficient labels is restricted. To address these limitations, we propose a novel generalist GAD paradigm that aims to develop a unified model capable of detecting anomalies on multiple unseen datasets without extensive retraining/fine-tuning or dataset-specific customization. To this end, we propose ARC, a few-shot generalist GAD method that leverages in-context learning and requires only a few labeled normal samples at inference time. Specifically, ARC consists of three core modules: a feature Alignment module to unify and align features across datasets, a Residual GNN encoder to capture dataset-agnostic anomaly representations, and a cross-attentive in-Context learning module to score anomalies using few-shot normal context. Building on ARC, we further introduce ARC_{zero} for the zero-shot generalist GAD setting, which selects representative pseudo-normal nodes via a pseudo-context mechanism and thus enables fully label-free inference on unseen datasets. Extensive experiments on 17 real-world graph datasets demonstrate that both ARC and ARC_{zero} effectively detect anomalies, exhibit strong generalization ability, and perform efficiently under few-shot and zero-shot settings.

Index Terms—Graph anomaly detection, foundation models, in-context learning, few-shot learning, zero-shot learning.

I. INTRODUCTION

GRAPH anomaly detection (GAD) aims to detect nodes that deviate significantly from the majority within a graph [1]–[6]. Since graph-structured data are ubiquitous in real-world domains such as finance, cybersecurity, e-commerce, and social networks, GAD holds significant practical value and has received widespread research attention [7], [8]. For example, in the domain of cybersecurity, GAD is commonly used to identify compromised devices or users within a network, such as detecting nodes exhibiting unusual communication patterns that could indicate network intrusions or insider threats [9].

Y. Liu, S. Li, Y. Zheng, and S. Pan are with the School of Information and Communication Technology, Griffith University, Australia.

Q. Chen is with the School of Computer, Electronics and Information, Guangxi University, Nanning, China.

C. Zhang is with the Department of Data Science and Artificial Intelligence, The Hong Kong Polytechnic University, Hong Kong.

P. S. Yu is with the Department of Computer Science, University of Illinois at Chicago, Chicago, IL 60607-7053, USA.

Corresponding author: Shirui Pan (E-mail: s.pan@griffith.edu.au).

Y. Liu and S. Li contributed equally to this work.

With the breakthroughs in deep learning techniques, in recent years, graph neural networks (GNNs)-based GAD methods have emerged as the de facto solution and become the focus of extensive research [4], [5], [10]. The general pipeline of these methods involves training a GNN-based GAD model in a data-driven manner, allowing the model to predict an anomaly score for each node that indicates its level of abnormality [1]–[3]. Based on the availability of anomaly labels during training, existing methods can be categorized into two types: supervised GAD methods and unsupervised GAD methods. In supervised methods (Fig. 1(a)), the GNN-based GAD model is a binary classifier that is trained under the supervision of anomaly labels. With specialized architecture designs and objective functions, these GNN classifiers are highly effective at capturing anomaly patterns [3], [7], [11], [12]. Unlike supervised methods, unsupervised GAD methods (Fig. 1(b)) optimize the models using unsupervised learning techniques without using labels, and then estimate abnormality through carefully designed anomaly score functions [13]–[15].

Despite the great success afforded by current GAD methods, they typically follow **dataset-specific learning paradigms**: the GAD model is trained exclusively on a target dataset and is only effective for that dataset. Unfortunately, the inherent limitations of such “one-model-for-one-dataset” paradigms not only increase the training and data costs of GAD methods but also hinder their application to new scenarios. *Firstly*, training a dedicated model from scratch for each target dataset can result in high application costs, including training time and device usage, particularly for large-scale graph data. *Secondly*, training GAD models requires full access to the target dataset, and for supervised methods, sufficient labels are also necessary. This makes GAD models difficult to apply in privacy-sensitive scenarios (e.g., healthcare and finance) where data is usually inaccessible. *Thirdly*, it is non-trivial to select the “optimal” GAD method for each dataset, as the performance of GAD models varies across different datasets [12]. In such cases, one might need to experiment with various GAD approaches and carefully tuned hyperparameters to adapt to a new dataset, leading to more expensive application costs. Given the aforementioned limitations, we raise the core research question of this article:

Research Question: *Instead of learning dataset-specific GAD models, can we train a unified generalist GAD model that can be applied across multiple datasets without requiring extensive retraining or customization?*

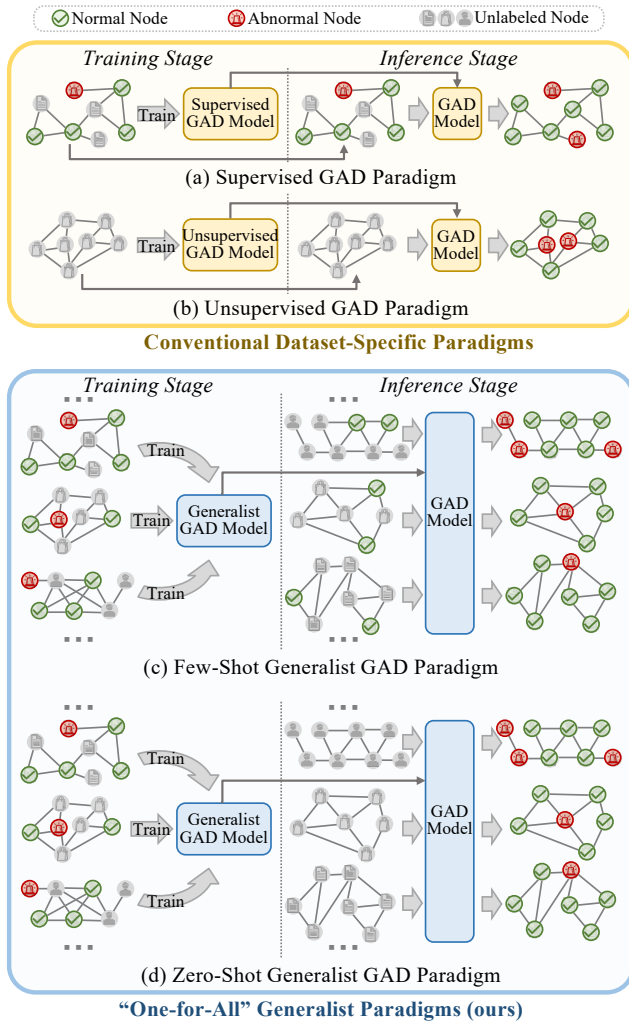


Fig. 1. The sketch maps of the existing data-specific GAD paradigms ((a) supervised and (b) unsupervised) and our generalist GAD paradigms ((c) few-shot and (d) zero-shot).

Following the recent research trend of foundation models and artificial general intelligence, a promising answer to this question is to develop a **generalist GAD method**. As illustrated in the blue block of Fig. 1, a generalist GAD model is trained on a collection of datasets, learning to capture anomaly patterns across various domains. Once it is well trained, the model can directly detect anomalies in any unseen dataset during the inference phase. The generalist learning paradigm, which has already proven effective in image anomaly detection [16] and link prediction [17], naturally avoids the limitations of the traditional approach. On the one hand, the generalist paradigm eliminates the need for full datasets and labels during training, enabling it to efficiently handle large-scale data and privacy-sensitive domains. On the other hand, it reduces the time and costs associated with data-specific model training and complex model selection, making it more adaptable and cost-effective for new scenarios.

According to the availability of labels in the target dataset, the generalist GAD problem can be divided into two types: few-shot and zero-shot settings [16], [18]. In the **few-shot** generalist GAD setting (Fig. 1(c)), the labels of *few-shot*

normal samples are available during inference time. These samples provide crucial guidance for the generalist GAD model, offering a reference for normal behaviors and insights into the characteristics of specific datasets. Note that the number of shots can be far fewer than what is typically required for supervised GAD, significantly reducing its application costs. In the **zero-shot** setting (Fig. 1(d)), differently, the generalist GAD model can detect anomalies without needing any labeled samples from the target dataset during inference. For the scenarios where annotation costs are extremely high, a zero-shot generalist GAD model can serve as a complementary approach to its few-shot counterpart, further expanding its applicability in real-world scenarios. Since both few-shot and zero-shot settings are commonly encountered in real-world applications, the goal of this paper is to develop effective solutions tailored to both of them.

While generalist GAD paradigms have strong applicability in real-world scenarios, designing an effective generalist GAD method remains a non-trivial task. Specifically, four key challenges arise, as outlined below:

- **Challenge 1 - feature diversity across different datasets.** Unlike image or language data where raw features are mapped into a unified space, in graph-structured data, the dimensionality and semantic space of node attributes can differ significantly across diverse datasets. In this case, aligning the features of different datasets at the input side of the generalist GAD model becomes a crucial challenge [19].
- **Challenge 2 - anomaly-aware representation encoding.** In a GAD model, the quality of anomaly-aware node-level representations is largely depends on the specific design of GNN architectures. In generalist settings, how to improve the GNN encoder to capture dataset-agnostic representations presents a significant challenge, as anomaly patterns can vary greatly across different datasets.
- **Challenge 3 - few-shot normal sample-guided detection.** Under the conventional paradigms, existing GAD methods can effectively learn how to identify anomalies through dataset-specific training. However, a few-shot generalist GAD model is expected to detect anomalies with minimal labeled samples and without model optimization, necessitating the design of models that can effectively leverage the limited few-shot normal samples.
- **Challenge 4 - pattern identification in zero-shot scenarios.** In the zero-shot setting, the generalist GAD model cannot rely on any labeled samples to obtain information about the data characteristics and distribution of the target dataset. Under this circumstance, accurately recognizing and capturing these characteristics becomes a significant challenge in designing an effective zero-shot method.

To tackle these challenges, in this work¹, we take a pioneering step in studying the generalist GAD problem. We propose ARC and ARC_{zero}, two effective generalist GAD methods tailored for the few-shot and zero-shot paradigms, respectively. Specifically, we first present the few-shot method ARC which is composed of three well-crafted modules. To solve **Challenge 1**,

¹It is an extension and re-innovation to our conference article [20] accepted by NeurIPS 2024.

we design a smoothness-based feature **A**lignment module. The alignment module first unifies the feature dimensions of different datasets using linear projections, and then aligns their semantic space by employing a smoothness-based reordering technique to ensure consistency across datasets. To address **Challenge 2**, we propose an ego-neighbor **R**esidual GNN as our encoder. Employing a specialized multi-hop residual architecture, the encoder learns anomaly-aware representations that capture both high-order affinity and heterophily in diverse datasets. To deal with **Challenge 3**, we design a cross-attentive in-Context anomaly scoring module. A cross-attention block is established to reconstruct the representations of unlabeled nodes using the representations of few-shot normal nodes (denoted as context nodes). The reconstruction error for each node is then used as its anomaly score, allowing ARC to make predictions in an in-context learning manner. Last but not least, to address **Challenge 4**, we propose ARC_{zero} , a zero-shot generalist GAD method that builds upon and extends the framework of ARC. In ARC_{zero} , we introduce a pseudo-context mechanism that automatically and iteratively selects the most representative samples to act as context nodes in ARC. This self-learning approach allows the model to capture dataset characteristics without any labeled data, enabling effective zero-shot anomaly detection. In summary, the primary contributions of this work are as follows:

- **New research problem.** We formulate and investigate the generalist GAD problem, which is an important yet under-explored direction. We further introduce two generalist GAD paradigms (few-shot and zero-shot), which model different real-world scenarios with varying levels of label availability.
- **Few-shot solution.** Aiming at the few-shot generalist GAD problem, we propose a novel method ARC. With carefully designed alignment, encoding, and in-context learning modules, ARC can efficiently detect anomalies in unseen graphs on the fly using only a few shots of normal samples.
- **Zero-shot solution.** For the more challenging zero-shot problem, we further propose ARC_{zero} , which enhances ARC by incorporating a pseudo-context mechanism. ARC_{zero} can automatically identify representative samples as context nodes, enabling zero-shot detection in new datasets.
- **Extensive experiments.** We conduct extensive experiments on 17 real-world graph datasets (4 for training and 13 for evaluation), and the experimental results indicate the anomaly detection performance, out-of-domain generalization ability, running efficiency, and few-shot/zero-shot capability of ARC and ARC_{zero} .

This work significantly extends our preliminary paper published in NeurIPS conference [20] by providing sufficient improvements in several key aspects: 1) We formulate the generalist GAD problem into a finer-grained taxonomy, categorizing it into few-shot and zero-shot settings. These new settings align with real-world constraints on label availability and application scenarios, making them more practical for diverse anomaly detection tasks. 2) We propose a novel method ARC_{zero} for zero-shot generalist GAD problem. Extensive experiments verify the superior zero-shot performance of ARC. 3) We provide a more in-depth analysis and discussion of the design

motivation and underlying mechanisms of ARC and ARC_{zero} . 4) We conduct more experiments to discuss the performance and characteristics of the proposed methods, including out-of-domain generalization experiments, detailed ablation studies, parameter analysis, and visualization.

II. RELATED WORKS

A. Anomaly Detection

Anomaly detection (AD) aims to identify instances that deviate significantly from the norm [21]. Due to limited anomaly labels, most AD methods operate in unsupervised settings [22], [23], including one-class modeling [22], reconstruction-based approaches [24], and distance/generative/self-supervised techniques [25]–[27]. Recently, large language models (LLMs) and visual-language models (VLMs) also show potential in addressing AD tasks [28], [29].

However, most AD methods are dataset-specific, limiting generalization to unseen domains. Generalist AD targets a single model that transfers to new datasets without retraining [16], [30], e.g., InCTRL using pre-trained VLMs [16]. While the above methods focus on generalist AD for image data, in this paper, we propose the first generalist AD method for graph-structured data.

B. Graph Anomaly Detection

Graph anomaly detection (GAD) aims to identify entities that deviate from the majority in graphs [3], [12]. In this paper, we focus on node-level detection [5]. While early studies used shallow mechanisms (e.g., residual analysis) [31], [32], recent approaches predominantly rely on graph neural networks (GNNs) [3], [4], which can be broadly categorized into supervised and unsupervised GAD methods [5], [12]. Supervised GAD formulates detection as binary classification and improves GNN aggregation/architecture/losses for anomaly patterns [3], [7], [11], [33], e.g., BWGNN with band-pass filters and GHRN with high-frequency pruning [3], [11]. Since labels are often unavailable, unsupervised GAD methods detect anomalies without annotated labels [2], [34]–[36]. Representative approaches include reconstruction-based methods such as DOMINANT [1], contrastive learning methods such as CoLA [2], and affinity-based methods such as TAM [10].

Although the methods mentioned above can detect anomalies in the training dataset, they are typically “one-for-one”: a separate model (and often dataset-specific training/validation) is required for each target graph, which limits their applicability to new and unseen domains. In contrast, cross-domain and transfer-learning GAD aim to improve generalization across domains by leveraging a source domain and adapting to a specific target domain, where target-domain adaptation or fine-tuning is commonly involved [37], [38]. However, these settings still assume access to the target domain and do not directly support on-the-fly deployment to arbitrary unseen graphs.

Motivated by this gap, we study generalist GAD, which trains a single model on a collection of graphs and directly deploys it to unseen graphs without any dataset-specific fine-tuning. Very recently, AnomalyGFM [39] and UNPrompt [18]

explore generalist GAD by leveraging GAD-oriented foundation modeling and unified neighborhood prompts, respectively. Nonetheless, their performance can be sensitive to design choices and hyperparameter settings across datasets, which may hinder truly prior-free deployment to new domains. To address this, ARC [20] proposes an attention-based in-context learning mechanism for few-shot generalist GAD with a small set of normal nodes at inference time, and we further develop ARC_{zero} to remove this requirement by constructing a pseudo-context and refining it iteratively with multi-round aggregation for reliable zero-shot anomaly scoring.

C. In-Context Learning

In-context learning (ICL) adapts a model at inference time using context examples, without explicit retraining [40]. It has shown effectiveness in natural language processing and vision, and is widely used in few-shot/zero-shot settings [41], [42]. Recent work extends ICL to graphs, e.g., prompt graphs for node/edge tasks [43] and universal link prediction with contextual cues [17]. However, they typically assume a multi-class context at inference, whereas generalist GAD needs a one-class (normal) context; our attention-based ICL mechanism addresses this and further supports zero-shot detection via pseudo-context refinement.

III. BACKGROUND AND PROBLEM STATEMENT

A. Notations

Throughout this paper, we use bold lowercase letters (e.g. \mathbf{a}), bold uppercase letters (e.g. \mathbf{A}), and calligraphic fonts (e.g. \mathcal{A}) to denote vectors, matrices, and sets, respectively.

We denote an undirected and attributed graph as $G = (\mathcal{V}, \mathcal{E}, \mathbf{X})$, where $\mathcal{V} = \{v_1, \dots, v_n\}$ is the node set with n nodes, \mathcal{E} is the edge set with m edges, and $\mathbf{X} \in \mathbb{R}^{n \times d}$ is the feature matrix where the i -th row \mathbf{x}_i is the feature vector for node v_i . The graph structure can be represented by a binary adjacency matrix $\mathbf{A} \in \{0, 1\}^{n \times n}$, where the i, j -th entry $a_{i,j} = 1$ indicates that v_i and v_j , otherwise $a_{i,j} = 0$.

In the context of anomaly detection (GAD) tasks, the node set can be written by $\mathcal{V} = \mathcal{V}_a \cup \mathcal{V}_n$ (satisfying $\mathcal{V}_a \cap \mathcal{V}_n = \emptyset$), where \mathcal{V}_a and \mathcal{V}_n are the abnormal node set and normal node set, respectively. Typically, the number of anomalies is far less than that of normal nodes, i.e., $|\mathcal{V}_a| \ll |\mathcal{V}_n|$. A label vector $\mathbf{y} \in \{0, 1\}^n$ can be used to describe node abnormality, where the i -th element $y_i = 1$ iff $v_i \in \mathcal{V}_a$ and $y_i = 0$ iff $v_i \in \mathcal{V}_n$.

B. Problem definition

Definition 1 (Dataset-Specific GAD Problem). Given graph $G = (\mathcal{V}, \mathcal{E}, \mathbf{X})$, the objective of dataset-specific GAD is to learn an anomaly scoring function (i.e., GAD model) $f : \mathcal{V} \rightarrow \mathbb{R}$ such that $f(v') > f(v)$ for $\forall v' \in \mathcal{V}_a$ and $\forall v \in \mathcal{V}_n$. The GAD model f is optimized on the dataset $\mathcal{D} = (G, \mathbf{y})$ during the training phase and is then used solely to predict the abnormality of nodes in the same dataset \mathcal{D} during the inference phase. For supervised GAD methods, the labels of a fraction of nodes are available for training, while unsupervised GAD methods solely learn from the unlabeled graph G .

The conventional data-specific setting follows the paradigm of “one-model-for-one-dataset”, which comes with several inherent limitations such as high training costs, excessive data requirements, and poor generalization ability. To address these limitations, this paper investigates the generalist GAD problem, aiming to develop a unified generalist model that can be directly applied to multiple and diverse datasets. Specifically, the generalist GAD problem can be written as:

Definition 2 (Generalist GAD Problem). We define $\mathcal{T}_{train} = \{\mathcal{D}_{train}^{(1)}, \dots, \mathcal{D}_{train}^{(N)}\}$ as a collection of training datasets, where each $\mathcal{D}_{train}^{(i)} = (\mathcal{G}_{train}^{(i)}, \mathbf{y}_{train}^{(i)})$ is a labeled dataset from an arbitrary domain. Similarly, a collection of testing datasets can be defined as $\mathcal{T}_{test} = \{\mathcal{D}_{test}^{(1)}, \dots, \mathcal{D}_{test}^{(N')}\}$, where each graph may come from a different domain. Note that there is no overlap between two collections, i.e. $\mathcal{T}_{train} \cap \mathcal{T}_{test} = \emptyset$. The objective of generalist GAD is to train a generalist GAD model f on \mathcal{T}_{train} , so that f can identify anomalies in any testing dataset $\mathcal{D}_{test}^{(i)} \in \mathcal{T}_{test}$, without the need for dataset-specific re-training or fine-tuning.

According to the availability of the labels of testing datasets during inference, the generalist GAD problem can be further divided into two categories: **few-shot** generalist GAD and **zero-shot** generalist GAD. In the few-shot setting, a small number of normal node labels from each dataset $\mathcal{D}_{test}^{(i)}$ are available during inference [16]. In the zero-shot setting, the labels of the testing dataset are completely inaccessible to the GAD model, making it more challenging than its few-shot counterpart [18]. In this paper, we propose simple yet effective solutions — ARC and ARC_{zero} — to address both settings, respectively.

IV. ARC: A FEW-SHOT GENERALIST GAD APPROACH

In this section, we introduce ARC, a few-shot generalist GAD approach. As illustrated by the pipeline (a)→(b)→(c) in Fig. 2, ARC is composed of three core modules: smoothness-based feature alignment, ego-neighbor residual graph encoder, and cross-attentive in-context anomaly scoring. In the initial step, we align the features from various datasets through projection and sorting, ensuring consistency in both dimensionality and semantics. Subsequently, a residual GNN with multi-hop information aggregation is employed to capture the representation of each node. Finally, a cross-attentive anomaly scoring module reconstructs the representations of query nodes (i.e., unlabeled nodes) by leveraging the representations of context nodes (i.e., few-shot normal nodes) through a cross-attention block, where the reconstruction errors finally serve as the predicted anomaly scores. In the following subsections, we provide a detailed introduction to the algorithmic design of each module in ARC.

A. Smoothness-Based Feature Alignment

A primary requirement for establishing a generalist and universal model for multiple datasets is that they share a unified input space. For example, in computer vision tasks, images are typically represented as pixel grids with consistent dimensionality, and in natural language processing, texts are tokenized into a common vocabulary space. Unlike these

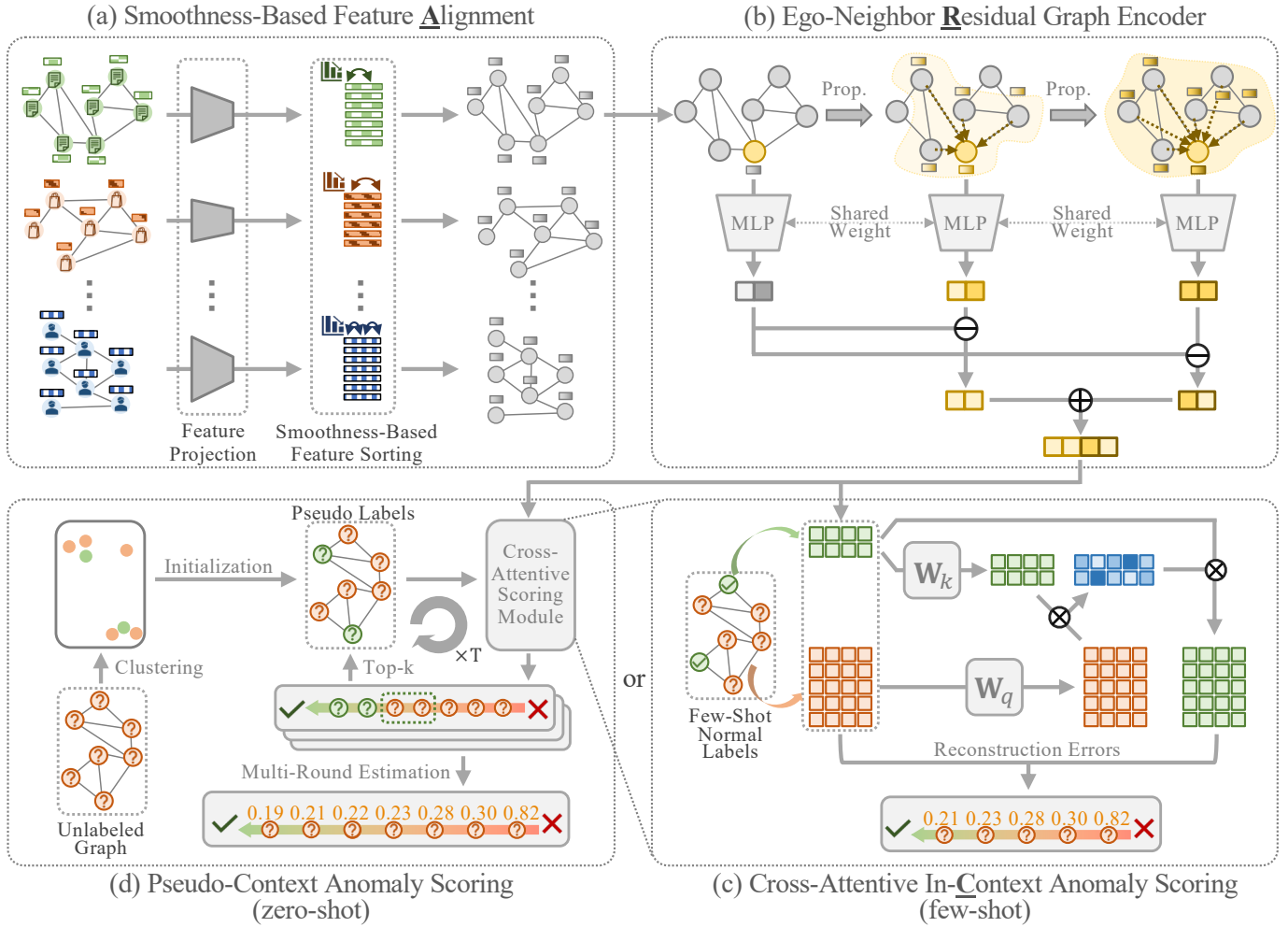


Fig. 2. The overall pipeline of the proposed methods ARC, illustrating by (a)→(b)→(c), and ARC_{zero} , illustrating by (a)→(b)→(d).

scenarios, in graph-structured data, the vectorized node features from different datasets often exhibit varying dimensions and belong to distinct semantic spaces. For instance, a social network dataset might have nodes with social attributes like age and profession, while an e-commerce network could feature nodes with attributes such as purchase frequency and average spending. To alleviate this feature heterogeneity, the first step in our generalist GAD method is to align the features of different datasets by standardizing their dimensionality and semantic space. Specifically, the dimensionality is unified using a linear feature projection, while the semantic space alignment is achieved through smoothness-based feature sorting, which will be demonstrated as follows.

1) *Linear Feature Projection*: To align the dimensionality of features from different graph datasets, we employ a dataset-specific linear feature projection for each of them. Concretely, given a feature matrix $\mathbf{X}^{(i)} \in \mathbb{R}^{n^{(i)} \times d^{(i)}}$ from $\mathcal{D}^{(i)} \in \mathcal{T}_{\text{train}} \cup \mathcal{T}_{\text{test}}$, a linear mapping is applied to project the feature into a unified dimension d_u :

$$\tilde{\mathbf{X}}^{(i)} = \text{Proj}(\mathbf{X}^{(i)}) = \mathbf{X}^{(i)} \mathbf{W}^{(i)}, \quad (1)$$

where $\tilde{\mathbf{X}}^{(i)} \in \mathbb{R}^{n^{(i)} \times d_u}$ is the projected feature matrix for $\mathcal{D}^{(i)}$ and $\mathbf{W}^{(i)} \in \mathbb{R}^{d^{(i)} \times d_u}$ is a dataset-specific linear projection

weight matrix.

A straightforward strategy is to utilize learnable linear mappings to optimize the projection weight matrix for each dataset. However, this approach introduces additional fine-tuning costs for testing datasets, which contradicts the core principle of generalist GAD paradigms. Therefore, to avoid test-time training while maintaining model generality, we employ principal component analysis (PCA) [44], a widely used dimensionality reduction method, to conduct the linear mapping. Projecting the features with PCA not only reduces the application costs on testing datasets but also ensures the most informative components of the features across different datasets are captured.

2) *Smoothness-based Feature Sorting*: After unifying the dimensionality, the next step is to align the feature semantic space across different datasets. To achieve this, one potential approach is to leverage pre-trained language models or large language models (LLMs) to map the features into a common semantic space [45]. Nevertheless, the language model-based strategies require the node features to be naturally represented as texts, which may restrict their applicability to certain types of datasets, especially when node features are non-textual or highly structured, such as numerical or categorical data [19].

Considering the difficulty of semantic-level feature matching,

in ARC, we explore an alternative pathway: *aligning features based on their contribution to the anomaly detection task*. Concretely, we measure the intrinsic importance of specific features for anomaly detection and reorder the permutation of features based on the measured significance. In this way, the features from different datasets can be semantically aligned in a task-sensitive manner, ensuring that the downstream encoder and scoring modules can distinguish and effectively process features with varying contributions to anomaly detection.

Smoothness as Contribution Measurement. To evaluate the feature contribution to GAD, a simple and dataset-agnostic measurement is desired. Motivated by its correlations to graph spectral and spatial properties [3], [11], we propose **feature-level smoothness** as a key criterion for evaluating feature importance. Formally, given $\mathcal{G} = (\mathcal{V}, \mathcal{E}, \mathbf{X})$ with a normalized feature matrix \mathbf{X} , the smoothness of the k -th feature dimension can be formulated by:

$$s_k(\mathbf{X}) = -\frac{1}{|\mathcal{E}|} \sum_{(v_i, v_j) \in \mathcal{E}} (\mathbf{X}_{ik} - \mathbf{X}_{jk})^2, \quad (2)$$

where a smaller value of s_k indicates a more significant change in the k -th feature between connected nodes in a graph.

Theoretically, we can understand the significance of smoothness to GAD tasks from both spectral and spatial perspectives. From a spectral perspective, the inverse of the low-frequency energy ratio is positively correlated with the node-level anomaly degree, as suggested in [3]. This means that a high-frequency graph signal (i.e., graph feature) can contribute more to indicating the presence of anomalies. Mathematically, let $\mathbf{x}_k = \mathbf{X}_{\cdot k}$ and $\mathbf{L} = \mathbf{D} - \mathbf{A}$ be the combinatorial graph Laplacian. Since $\mathbf{x}_k^\top \mathbf{L} \mathbf{x}_k = \frac{1}{2} \sum_{(v_i, v_j) \in \mathcal{E}} (\mathbf{X}_{ik} - \mathbf{X}_{jk})^2$, our smoothness metric is equivalent to the negative normalized Dirichlet energy: $s_k(\mathbf{X}) = -\frac{2}{|\mathcal{E}|} \mathbf{x}_k^\top \mathbf{L} \mathbf{x}_k$. Using the spectral decomposition $\mathbf{L} = \mathbf{U} \mathbf{\Lambda} \mathbf{U}^\top$, we have $\mathbf{x}_k^\top \mathbf{L} \mathbf{x}_k = \sum_r \lambda_r \langle \mathbf{u}_r, \mathbf{x}_k \rangle^2$. This implies that a lower smoothness score s_k corresponds to higher energy in high-frequency spectral components [46], which are typically indicative of local anomalies. From a spatial perspective, smoothness reflects the local homophily and heterophily of features among neighboring nodes, as the definitions of homophily rate and smoothness are similar [47]. Since heterophily properties are highly indicative in discriminating anomalies [10], [11], smoothness serves as a useful metric for evaluating the discriminative power of features in GAD tasks.

Empirically, we design a motivating experiment to validate the correlation between a feature’s smoothness and its contribution to GAD tasks. During the data preprocessing phase, we calculate s_k of each raw feature dimension and sort the features in descending order. Based on this sorted order, we partition the features into five groups of subsets, corresponding to the percentiles 80%-100%, 60%-80%, \dots , and 0%-20%. We evaluate the anomaly detection performance of three mainstream GAD methods (DOMINANT [1], CoLA [2], and TAM [10]) by using each subset of features as input, and the results are shown in Fig. 3. On all four datasets, a consistent trend emerges: feature subsets with lower s_k demonstrate greater effectiveness in discriminating anomalies. In light of this, smoothness has been shown to be an effective

anomaly-related indicator for evaluating the relevance of each feature in different datasets.

Smoothness-based Sorting. In ARC, we utilize feature-level smoothness as a metric to reorder the projected features, facilitating task-oriented semantic alignment across datasets. Given the projected feature matrix $\tilde{\mathbf{X}}^{(i)}$, we first calculate the smoothness $s_k(\tilde{\mathbf{X}}^{(i)})$ of each column and then reorder the columns in descending order of their smoothness. The reordered feature matrix, denoted by $\mathbf{X}'^{(i)}$, serves as the aligned feature matrix for the graph dataset $\mathcal{D}^{(i)}$ and is fed into the encoder.

With the alignment strategy, we ensure that the first-column feature of all datasets is the one with the lowest smoothness, which may have the greatest contribution to the GAD predictions; in contrast, features with higher smoothness will appear in later columns, as they are less critical for anomaly detection. Taking the aligned features as input, the downstream encoder and scoring modules can learn to prioritize and effectively process the most relevant features for anomaly detection. Once a testing dataset is aligned in the same manner, the knowledge and capability of anomaly detection can be seamlessly transferred to this unseen dataset.

B. Ego-Neighbor Residual Graph Encoder

As the core component of a GAD method, the GNN-based encoder plays a pivotal role in learning representation for each node, capturing structural and semantic information of nodes to support effective anomaly detection. While conventional GNN models (e.g., GCN [48] and GAT [49]) perform well on tasks like classification and clustering, they do not inherently capture the nuanced patterns (e.g., high-frequency signals and heterophily) required for anomaly detection, often leading to sub-optimal performance [12]. While recent studies have developed specialized GNN architectures for supervised GAD, they are designed for dataset-specific scenarios rather than generalist GAD problems. For generalist scenarios, how to construct a GNN encoder that can capture transferable knowledge across domains remains an open problem.

In this paper, we propose an ego-neighbor residual graph encoder (RGE for short) to learn representations in generalist GAD scenarios. Combining a multi-hop mixing architecture and a residual operation, RGE is able to capture transferable and anomaly-sensitive knowledge on different datasets. As shown in Fig. 2(b), RGE employs a “propagation-then-transformation” design, which is similar to SGC [50]. Given the input feature matrix $\mathbf{X}^{[0]}$ (here $\mathbf{X}^{[0]}$ is the aligned feature \mathbf{X}' for each dataset), RGE first propagates the node features along the graph structure for L iterations, and then applies a shared MLP to perform non-linear transformations on both the initial and propagated features:

$$\mathbf{X}^{[l]} = \tilde{\mathbf{A}} \mathbf{X}^{[l-1]}, \quad \mathbf{Z}^{[l]} = \text{MLP}(\mathbf{X}^{[l]}), \quad (3)$$

where $l \in \{0, \dots, L\}$ is the iteration index, $\mathbf{X}^{[l]}$ is the propagated feature matrix at the l -th iteration, $\mathbf{Z}^{[l]}$ is the transformed representation matrix at the l -th iteration, and $\tilde{\mathbf{A}}$ is the normalized adjacency matrix [48], [50]. To fully leverage the information at different receptive fields, RGE learns

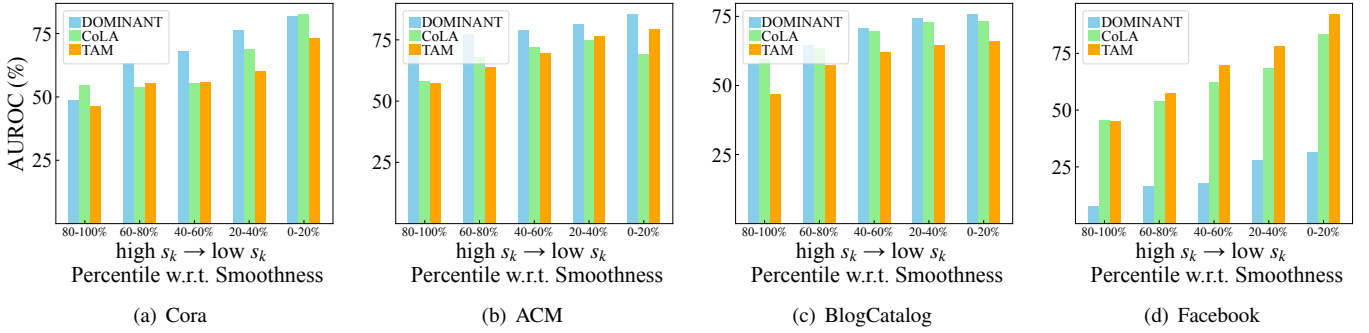


Fig. 3. AUROC on data with 5 groups of feature subsets.

representations from the initial features and all intermediate propagated features, which allows ARC to identify varied anomaly patterns from different datasets. Moreover, we utilize a shared MLP for transformation at all iterations, ensuring that the propagated features are consistently mapped into a unified representation space and preserving low computational costs.

After computing the transformed representations at different propagation steps, i.e., $\mathbf{Z}^{[0]}, \dots, \mathbf{Z}^{[L]}$, residual operations are applied to model the ego-neighbor differences. To be more specific, for each transformed representation matrix $\mathbf{Z}^{[l]}$ ($1 \leq l \leq L$), a residual representation matrix is obtained by calculating the difference between $\mathbf{Z}^{[l]}$ and the ego transformed representation matrix $\mathbf{Z}^{[0]}$ as follows:

$$\mathbf{R}^{[l]} = \mathbf{Z}^{[l]} - \mathbf{Z}^{[0]} \quad l \in \{1, \dots, L\}, \quad (4)$$

where $\mathbf{R}^{[l]}$ is the residual matrix at the l -th propagated iteration. The residual operation is the key design of RGE, allowing ARC to effectively learn representations that are highly sensitive to anomalies. *Firstly*, the residual operation emphasizes the differences between each node and its neighbors, explicitly modeling local affinity through the learned embeddings [10]. Since local affinity can effectively reflect node-level abnormalities [2], [10], the residual representations can capture these distinctive features for the downstream anomaly scoring module. *Secondly*, the first-order residual operation ($\mathbf{R}^{[1]}$) can be seen as a high-pass filter on the graph data, functioning similarly to a graph convolution with the graph Laplacian, a well-known high-pass operator on graphs [46], [48]. High-pass filters are effective in capturing high-frequency signals and local heterophily, both of which are valuable for detecting anomalies in GAD [3], [11], [51]. *Thirdly*, the residual operation has also been shown to be effective in shallow GAD methods (e.g., Radar [31]), further supporting its utility in capturing anomaly-related features. Unlike shallow methods, RGE can adaptively learn transformations and capture higher-order residual information through the multi-hop residual design, which enhances its modeling capacity and enables it to better capture complex anomaly patterns.

Once the residual representations are obtained at multiple iterations, RGE generates the final representations by concatenating them, which can be written by:

$$\mathbf{H} = [\mathbf{R}^{[1]} \parallel \dots \parallel \mathbf{R}^{[L]}], \quad (5)$$

where $\mathbf{H} \in \mathbb{R}^{n \times d_e}$ is the representation matrix and \parallel is the concatenation operator. By combining the residual information from different propagation steps, RGE can learn more comprehensive and anomaly-sensitive representations that capture patterns from diverse receptive fields. This is particularly beneficial for generalist GAD problems, as the anomaly patterns in datasets from different domains may span varying ranges of neighbors.

C. Cross-Attentive In-Context Anomaly Scoring

As the final stage of the pipeline of ARC, the cross-attentive in-context anomaly scoring module aims to predict the abnormality (i.e., anomaly scores) of each unlabeled node based on the few-shot normal nodes. Unlike existing supervised or unsupervised GAD scenarios, generalist GAD scenarios require the model to make direct predictions during the testing phase based solely on the provided few-shot normal samples, without the need for dataset-specific fine-tuning or additional training. In this context, how to effectively leverage the few-shot normal nodes becomes crucial for making accurate predictions.

To address this challenge, we propose a novel scoring module with a cross-attention mechanism for anomaly prediction based on the *in-context learning paradigm*. Following this paradigm, we denote the few-shot normal nodes as **context nodes** \mathcal{V}_k , while the remaining unlabeled nodes are denoted as **query nodes** \mathcal{V}_q that need to be predicted as anomalous or normal. In this setup, we split the representation matrix $\mathbf{H} \in \mathbb{R}^{n \times d_e}$ into two parts by indexing the corresponding row vectors: the representations of context nodes $\mathbf{H}_k \in \mathbb{R}^{n_k \times d_e}$ and the representations of query nodes $\mathbf{H}_q \in \mathbb{R}^{n_q \times d_e}$. Note that the number of context nodes n_k can be much smaller than the number of query nodes n_q in the few-shot setting.

The core idea of our in-context learning module is to reconstruct each query node representation with the combination of context node representations. Then, the reconstruction error of each query node can serve as its anomaly score to measure its abnormality. To this end, we design a value-free cross-attention block for reconstruction, where each row vector of \mathbf{H}_q (i.e., the representation of each query node) is represented through a linear combination of \mathbf{H}_k :

$$\begin{aligned} \mathbf{Q} &= \mathbf{H}_q \mathbf{W}_q, & \mathbf{K} &= \mathbf{H}_k \mathbf{W}_k, \\ \tilde{\mathbf{H}}_q &= \text{Softmax} \left(\frac{\mathbf{Q} \mathbf{K}^\top}{\sqrt{d_e}} \right) \mathbf{H}_k. \end{aligned} \quad (6)$$

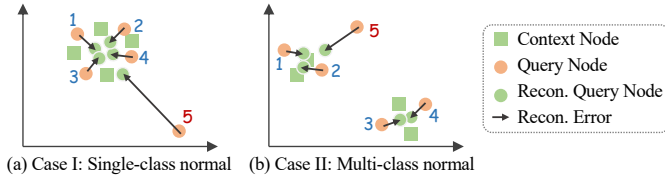


Fig. 4. Toy examples of reconstruction-based scoring mechanism. In each case, nodes 1, 2, 3, and 4 are normal samples, while node 5 is an anomaly.

where $\mathbf{Q} \in \mathbb{R}^{n_q \times d_e}$ and $\mathbf{K} \in \mathbb{R}^{n_k \times d_e}$ are the query and key matrices respectively, \mathbf{W}_q and \mathbf{W}_k are learnable parameters, and $\tilde{\mathbf{H}}_q \in \mathbb{R}^{n_q \times d_e}$ is the reconstructed query embedding matrix. Different from the cross-attention blocks in most models [52], [53], the value-free cross-attention block in ARC directly multiplies the attention matrix with \mathbf{H}_k , without mapping \mathbf{H}_k with an extra value matrix. In this way, we can ensure that $\tilde{\mathbf{H}}_q$ lies in the same representation space as \mathbf{H}_q , allowing the cross-attention block to perform reconstruction effectively. Given a query node v_i , we can predict its anomaly score $f(v_i)$ by calculating the L2 distance between its query representation vector $\mathbf{H}q_i$ and the corresponding reconstructed query representation vector $\tilde{\mathbf{H}}q_i$, which can be written by:

$$f(v_i) = d(\mathbf{H}q_i, \tilde{\mathbf{H}}q_i) = \sqrt{\sum_{j=1}^{d_e} (\mathbf{H}q_{ij} - \tilde{\mathbf{H}}q_{ij})^2}. \quad (7)$$

Mechanism Analysis. The design of the in-context anomaly scoring module is based on an assumption: The normal query nodes exhibit similar patterns to several context nodes, due to the inherent shared attributes within normal samples. As a result, their representations can be easily reconstructed by a linear combination of the context node representations. That is, given a normal node, its original and reconstructed representations can be close to each other in the representation space, leading to a smaller anomaly score $f(v_i)$. Conversely, since anomalies usually exhibit patterns that differ from those of normal nodes, it would not be easy to construct them using contextual normal nodes. Therefore, their reconstruction errors may be relevantly larger, resulting in higher anomaly scores.

To further illustrate the reconstruction-based scoring mechanism, we present two toy examples demonstrating how the reconstruction error functions as a measure of abnormality in different GAD scenarios. As shown in Fig. 4, we consider two typical scenarios: Case I - single-class normal, where all normal samples exhibit similar patterns or characteristics, and Case II - multi-class normal, where normal samples are grouped into multiple classes, each characterized by distinct patterns or traits. In Case I (Fig. 4(a)), we can witness that the normal query nodes stay in the same cluster with the context nodes, leading to their significantly smaller reconstruction errors compared to the abnormal node. Interestingly, if the cross-attention block assigns uniform weights to all context nodes, our scoring module can function as a one-class classification model [22], where the average of the context node representations is the one-class centroid. This inherent similarity between our scoring module and traditional anomaly detection methods ensures

compatibility and facilitates knowledge transfer across diverse anomaly detection scenarios. The toy example of Case II (Fig. 4(b)) further illustrates that our cross-attentive scoring module effectively handles the multi-class normal scenario. Specifically, given a normal query node, the cross-attention block can automatically identify and utilize the closest context samples belonging to the same cluster for reconstruction.

Model Training. To train ARC in an end-to-end manner, we utilize a marginal cosine similarity loss to minimize the reconstruction errors of normal nodes, while maximizing the reconstruction errors of abnormal nodes. In practice, for a training graph dataset with anomaly labels, we randomly select n_k normal nodes as context nodes and sample an equal number of normal and abnormal nodes to serve as query nodes. Given a query node v_i with representation $\mathbf{h}q_i$, reconstructed representation $\tilde{\mathbf{h}}q_i$, and anomaly label y_i , the sample-level loss function can be denoted as:

$$\mathcal{L} = \begin{cases} 1 - \cos(\mathbf{h}q_i, \tilde{\mathbf{h}}q_i), & \text{if } y_i = 0 \\ \max(0, \cos(\mathbf{h}q_i, \tilde{\mathbf{h}}q_i) - \epsilon), & \text{if } y_i = 1 \end{cases} \quad (8)$$

where $\cos(\cdot, \cdot)$ and $\max(\cdot, \cdot)$ denote the cosine similarity and maximum operation and ϵ is a margin hyperparameter.

V. ARC_{ZERO}: TOWARDS ZERO-SHOT GENERALIST GAD

In the previous section, we propose ARC, an effective few-shot generalist GAD approach. Nevertheless, in certain specific application domains where labeling costs are high or expert knowledge is required, even a few-shot set of normal samples may not be available. To extend generalist GAD to these domains, a zero-shot generalist GAD method capable of detecting anomalies without relying on labeled samples becomes highly desirable. As we already have a strong few-shot method ARC, a natural question arises: *can we develop a zero-shot generalist GAD method based on a well-trained ARC model with minor specialized modifications?*

To apply ARC to the zero-shot setting, a promising approach is to select appropriate unlabeled nodes to serve as context nodes, making the entire process function effectively. Building on this idea, we propose ARC_{zero}, a zero-shot generalist GAD method that leverages a pseudo-context mechanism for zero-shot anomaly scoring. The pipeline of ARC is demonstrated by (a)→(b)→(d) in Fig. 2. Using the same alignment module, encoder, and training process as ARC, ARC_{zero} introduces a new pseudo-context anomaly scoring module that self-adaptively selects pseudo-normal nodes to facilitate zero-shot anomaly detection. In the first step, we utilize a clustering algorithm to initialize the pseudo labels of few-shot normal nodes. Then, we iteratively execute the cross-attentive scoring module using the pseudo labels as input and then select new pseudo-context nodes from the remaining non-pseudo nodes according to the estimated scores. To conduct stable and reliable zero-shot anomaly detection, we aggregate the results from multiple iterations and compute the final anomaly scores by synthesizing the multi-round predictions. The following subsections provide a detailed explanation of each component.

A. Pseudo-Context Initialization

The core idea of ARC_{zero} is to leverage pseudo-normal nodes to approximate context nodes for effective zero-shot generalist GAD. In this context, the first step is to initialize the pseudo-normal nodes, serving as the cold-start context for the subsequent process. To select the pseudo-normal nodes as the context samples, we consider two key principles: *representativeness* and *diversity*. Specifically, the former requires the selected nodes to reflect the overall distribution of normal samples, while the latter indicates that the pseudo-normal nodes can capture a wide range of variations within the data.

Following the above principles, we propose a clustering-based strategy for pseudo-context initialization. To be more concrete, a k -means clustering algorithm [54] is first applied to the aligned features of the target dataset, partitioning the nodes into k clusters, each represented by a centroid. In practice, we set the number of clusters equal to the number of context nodes, i.e., $k = n_k$. For the choice of n_k , we can monitor self-consistency proxies, such as the convergence of iterative pseudo-context refinement and the tail-to-body separation of anomaly scores, to make better n_k choices without performance validation. After clustering, we initialize the pseudo-normal nodes as the samples closest to the centroids of each cluster. The selected n_k nodes can serve as the context nodes in the cross-attentive in-context anomaly scoring module at the first zero-shot scoring iteration.

Despite the simplicity of our clustering-based initialization strategy, it adheres to our principles of representativeness and diversity. On the one hand, the selected nodes are located near the cluster centers, where data distribution density is usually high, thus ensuring their *representativeness* by capturing the dominant patterns within the dataset. On the other hand, the clustering-based initialization strategy ensures *diversity* by selecting nodes from different clusters, with each cluster typically representing distinct patterns or normal categories, thereby capturing a broader spectrum of variations in the dataset. Moreover, even in extreme cases where frequent anomalies are mistakenly included in the initial pseudo-context, the subsequent iterative refinement and multi-round aggregation can progressively mitigate the impact of this imperfect start.

B. Iterative Pseudo-Context Anomaly Scoring

Taking the initialized pseudo-normal nodes as input, the cross-attentive scoring module in ARC can now predict the abnormality of all nodes in a zero-shot manner. Nevertheless, the pseudo-normal nodes selected by the clustering algorithm may not adequately characterize the distribution of normal data; more critically, the selected nodes can even be noisy, i.e., anomaly nodes might be mistakenly selected as context nodes, which further compromises the reliability of the predictions. In order to generate more reliable anomaly scores, we adopt a multi-iteration approach to refine the pseudo-normal nodes and generate more reliable zero-shot GAD predictions. In each iteration, we utilize the pseudo-normal nodes to compute anomaly scores for the current step; these scores are then employed to select more representative pseudo-normal nodes for the next iteration.

Concretely, at the t -th iteration step, given a set of pseudo-normal nodes, we can separate the node set \mathcal{V} into pseudo context node set $\mathcal{V}_k^{[t]}$ and query node set $\mathcal{V}_q^{[t]} = \mathcal{V} \setminus \mathcal{V}_k^{[t]}$. Following the procedure in Section IV-C, the anomaly score $f(v_i)^{[t]}$ of each node $v_i \in \mathcal{V}_q^{[t]}$ can be estimated, which measures the abnormality of all the query nodes at the current step. After that, we can sample the “most normal nodes” from the query set as the new pseudo-normal nodes for the next iteration, enabling a refined representation of normal patterns for improved scoring in the following steps. In practice, we pick the nodes with top- k smallest anomaly scores as the new pseudo-normal nodes, which can be written by:

$$\mathcal{V}_k^{[t+1]} = \operatorname{argmin}_{v_i \in \mathcal{V}_q^{[t]}}^k \{f(v_i)^{[t]}\}, \quad (9)$$

where $\mathcal{V}_k^{[t+1]}$ can play the role of pseudo-normal (context) nodes in the next step (i.e. the $(t+1)$ -th iteration). By employing this iterative mechanism, the model refines the pseudo-normal nodes and anomaly predictions in a self-adaptive manner, improving the accuracy and robustness of the detection process.

C. Multi-Round Anomaly Score Estimation

After multiple iterations, the abnormality predictions based on different groups of refined pseudo-normal nodes can be obtained. A naive solution is to employ the scores at the final iteration as the final zero-shot GAD prediction. However, the GAD predictions from a single iteration are often sub-optimal and unreliable due to the selection bias of pseudo-normal nodes and the prediction bias inherent in zero-shot anomaly scoring. To mitigate the potential instability arising from imperfect pseudo-context initialization, in ARC_{zero} , we propose aggregating the anomaly scores across multiple iterations as the final output, collectively enhancing the reliability and robustness of anomaly detection. For the anomaly scores at each iteration, we first impute the scores of pseudo-normal nodes by assigning them the smallest score value from the current iteration. Formally, given $v_i \in \mathcal{V}_k^{[t]}$, we define:

$$f(v_i)^{[t]} = \min_{v_j \in \mathcal{V}_k^{[t]}} \{f(v_j)^{[t]}\}. \quad (10)$$

The final anomaly score for each node $v_i \in \mathcal{V}$ is obtained by calculating the average score across all iterations:

$$f(v_i) = \frac{1}{T} \sum_{t=1}^T f(v_i)^{[t]}. \quad (11)$$

The algorithm and complexity analysis of ARC_{zero} see Appendices C and B, respectively.

VI. EXPERIMENTS

A. Experimental Setup

1) *Datasets*: For comprehensive evaluations, we consider graph datasets spanning multiple domains, such as social media, academic, e-commerce, crowd-sourcing service, and finance, with either injected anomalies or real anomalies [2], [10], [12], [55]. We partition all datasets into a training set, $\mathcal{T}_{\text{train}}$, and a testing set, $\mathcal{T}_{\text{test}}$, ensuring there is no overlap between the two

TABLE I
THE STATISTICS OF DATASETS.

Dataset	\mathcal{T}_{train}	\mathcal{T}_{test}	#Nodes	#Edges	#Feat.	#Ano.
Citation network with injected anomalies						
Cora	-	✓	2,708	5,429	1,433	150
CiteSeer	-	✓	3,327	4,732	3,703	150
ACM	-	✓	16,484	71,980	8,337	597
PubMed	✓	-	19,717	44,338	500	600
Social network with injected anomalies						
BlogCatalog	-	✓	5,196	171,743	8,189	300
Flickr	✓	-	7,575	239,738	12,047	450
Social network with real anomalies						
Facebook	-	✓	1,081	55,104	576	25
Weibo	-	✓	8,405	407,963	400	868
Reddit	-	✓	10,984	168,016	64	366
Questions	✓	-	48,921	153,540	301	1,460
Co-review network with real anomalies						
Amazon	-	✓	10,244	175,608	25	693
YelpChi	✓	-	23,831	49,315	32	1,217
Out-of-domain datasets with injected anomalies						
Amazon-Photo	-	✓	7,650	238,162	745	450
Coauthor-CS	-	✓	18,333	163,788	6,805	600
Out-of-domain datasets with real anomalies						
Tolokers	-	✓	11,758	519,000	10	2,566
T-Finance	-	✓	39,357	21,222,543	10	1,803
Elliptic	-	✓	203,769	234,355	166	4,545

sets. Specifically, we first collect four basic groups of datasets: 1) citation network with injected anomalies, including Cora, CiteSeer, ACM, and PubMed [56], [57]; 2) social network with injected anomalies, including BlogCatalog and Flickr [58]; 3) social network with real anomalies, including Facebook, Weibo, Reddit, and Questions [59]–[61]; 4) co-review network with real anomalies, including Amazon and YelpChi [62], [63]. Within each group, we consider the largest dataset to be one of the training datasets \mathcal{T}_{train} , and the rest are regarded as the in-domain testing datasets. To verify the out-of-domain generalization ability of the proposed methods, we consider 5 out-of-domain datasets: Coauthor-CS, a co-author network [55]; Amazon-Photo, a co-purchase network [55]; Tolokers, a crowdsourcing service network [61]; T-Finance, a finance network [3]; and Elliptic, a payment flow network [64]. These out-of-domain datasets exhibit significant diversity compared to the training datasets, as they come from diverse, new, and unseen domains. The detailed statistics of the datasets are shown in Table I, with additional explanations provided in Appendix A.

2) *Baselines*: We compare the proposed methods with those previous state-of-the-art methods, which can be generally divided into two categories: supervised methods and unsupervised methods. The supervised baselines include two conventional GNNs, i.e., GCN [48] and GAT [49], and three state-of-the-art supervised GAD methods, i.e., BGNN [65], BWGNN [3], and GHRN [11]. The unsupervised methods comprise four representative approaches, each featuring a unique design, including the generative method DOMINANT [1], the contrastive method CoLA [2], the hop predictive method HCM-A [35], and the affinity-based method TAM [10]. In addition, we also compare with two very recent generalist GAD methods, AnomalyGFM [39] and UNPrompt [18], to evaluate the performance against the latest state-of-the-art.

3) *Evaluation Metrics*: Following previous studies [10], [12], we employ two popular and complementary evaluation

metrics for evaluation, including area under the receiver operating characteristic Curve (AUROC) and area under the precision-recall curve (AUPRC). A higher AUROC/AUPRC value indicates better performance. To ensure robustness, we report the average AUROC and AUPRC along with their standard deviations over 5 trials.

4) *Implementation Details*: To implement the generalist GAD settings, we train the baselines as well as the proposed methods on all the datasets in \mathcal{T}_{train} and evaluate them on each dataset in \mathcal{T}_{test} . During the inference phase, ARC performs predictions on each testing dataset using an in-context learning approach, with a default shot number of $n_k = 10$. For ARC_{zero} , we also set the number of pseudo-normal nodes as 10. For the supervised baselines, we train the models on \mathcal{T}_{train} and directly evaluate on each $\mathcal{D}_{test}^{(i)} \in \mathcal{T}_{test}$, since no labeled anomaly is available for fine-tuning (denoted as “pre-train only”). For the unsupervised baselines, we evaluate two settings: “pre-train only” and “pre-train & fine-tune”. In the latter setting, we perform additional dataset-specific fine-tuning for a few epochs. We standardized the testing samples for each dataset across different methods to ensure a fair comparison. To standardize the feature space in the baseline methods, we employ either a learnable projection or a random projection as an adapter between the raw features and the model’s input layer. We use random search to optimize the hyperparameters for both the baselines and the proposed methods. We avoid dataset-specific hyperparameter tuning to align with our goal of developing generalist GAD models. Instead, we apply a single set of hyperparameters for all testing datasets, i.e., using one unified hyperparameter configuration across all datasets (training and testing) without any dataset-specific tuning. Specifically, for ARC and ARC_{zero} , we fix the key hyperparameters (e.g., representation dimension $h = 64$, layer number $L = 2$, shot number $n_k = 10$) across all datasets. For the baselines, we conduct 50 trials of random search within their specific parameter spaces to ensure optimal performance.

B. Performance Comparison

The performance comparison on 13 testing datasets is summarized in Table II in terms of AUROC. The corresponding AUPRC results are reported in Appendix D. Based on the results, we have made the following observations regarding the proposed methods ARC and ARC_{zero} :

- **Superior performance.** The proposed ARC and ARC_{zero} consistently outperform baseline methods across nearly all datasets, as shown by their significantly higher AUROC and AUPRC scores. This highlights their ability to generalize to diverse datasets under the generalist GAD scenarios, achieving state-of-the-art performance for both supervised and unsupervised baselines. Moreover, compared to the latest generalist baselines (UNPrompt and AnomalyGFM), ARC_{zero} achieve consistently stronger overall performance, and the difference is statistically significant based on paired t-test and Wilcoxon signed-rank test ($p < 0.05$).
- **Less application costs.** Our methods achieve strong performance without requiring any dataset-specific fine-tuning, making them highly efficient and cost-effective for real-world

TABLE II

ANOMALY DETECTION PERFORMANCE IN TERMS OF AUROC (IN PERCENT, MEAN±STD). HIGHLIGHTED ARE THE RESULTS RANKED **FIRST**, **SECOND**, AND **THIRD**. “RANK” INDICATES THE AVERAGE RANKING OVER 13 DATASETS. SUPERSCRIP “*” ON A BASELINE METHOD NAME INDICATES THAT OUR METHOD IS SIGNIFICANTLY DIFFERENT FROM THIS BASELINE ON ALL_DATASETS_TRIAL_AVG (PAIRED T-TEST AND WILCOXON TEST, P<0.05).

Method	Cora	CiteSeer	ACM	BlogCatalog	Facebook	Weibo	Reddit
Supervised - Pre-Train Only							
GCN	59.64±8.30	60.27±8.11	60.49±9.65	56.19±6.39	29.51±4.86	76.64±17.69	50.43±4.41
GAT	50.06±2.65	51.59±3.49	48.79±2.73	50.40±2.80	51.88±2.16	53.06±7.48	51.78±4.04
BGNN	42.45±11.57	42.32±11.82	44.00±13.69	47.67±8.52	54.74±25.29	32.75±35.35	50.27±3.84
BWGNN	54.06±3.27	52.61±2.88	67.59±0.70	56.34±1.21	45.84±4.97	53.38±1.61	48.97±5.74
GHRN	59.89±6.57	56.04±9.19	55.65±6.37	57.64±3.48	44.81±8.06	51.87±14.18	46.22±2.33
Unsupervised - Pre-Train Only							
DOMINANT	66.53±1.15	69.47±2.02	70.08±2.34	74.25±0.65	51.01±0.78	92.88±0.32	50.05±4.92
CoLA	63.29±8.88	62.84±9.52	66.85±4.43	50.04±3.25	12.99±11.68	16.27±5.64	52.81±6.69
HCM-A	54.28±4.73	48.12±6.80	53.70±4.64	55.31±0.57	35.44±13.97	65.52±12.58	48.79±2.75
TAM	62.02±2.39	72.27±0.83	74.43±1.59	49.86±0.73	65.88±6.66	71.54±0.18	55.43±0.33
Unsupervised - Pre-Train & Fine-Tune							
DOMINANT	72.23±0.34	74.69±0.32	74.34±0.12	74.61±0.04	49.92±0.55	92.21±0.10	52.14±5.06
CoLA	67.62±4.26	70.75±3.42	69.11±0.67	62.49±3.38	64.70±18.86	31.55±6.02	58.12±0.67
HCM-A	56.45±4.93	55.54±4.07	57.69±3.59	55.10±0.29	36.57±10.72	71.89±2.79	49.15±2.72
TAM	62.56±2.10	76.54±1.33	86.29±1.57	57.69±0.88	76.26±3.70	71.73±0.16	56.62±0.49
Generalist							
UNPrompt*	67.02±3.06	72.84±1.95	74.93±0.84	68.80±0.18	78.46±4.91	48.52±0.86	56.75±0.84
AnomalyGFM*	50.67±2.90	50.63±3.07	51.13±2.53	45.89±0.39	87.58±3.41	66.31±8.12	55.93±3.62
ARC (ours)	87.45±0.74	90.95±0.59	79.88±0.28	74.76±0.06	67.56±1.60	88.85±0.14	60.04±0.69
ARC _{zero} (ours)	87.54±0.57	91.20±0.27	78.78±0.17	74.75±0.03	69.25±0.95	88.71±0.18	59.57±0.42
Method	Amazon	Amazon-Photo	Coauthor-CS	Tolokers	T-Finance	Elliptic	Avg. Rank
Supervised - Pre-Train Only							
GCN	46.63±3.47	59.27±1.00	63.79±0.68	53.38±3.29	58.79±8.50	51.88±6.81	9.2
GAT	50.52±17.22	52.80±10.08	50.16±3.38	46.23±11.95	45.05±14.44	57.38±7.14	12.1
BGNN	52.26±3.31	58.69±3.06	63.25±0.70	48.44±8.27	50.97±1.15	51.70±2.09	12.2
BWGNN	55.26±16.95	55.55±7.47	59.45±11.12	44.85±9.24	52.19±23.09	55.55±6.25	11.1
GHRN	49.48±17.13	56.18±1.83	68.64±0.83	59.53±6.61	54.43±10.62	54.39±5.70	9.8
Unsupervised - Pre-Train Only							
DOMINANT	48.94±2.69	47.39±1.20	60.61±0.52	48.12±4.85	OOM	OOM	10.2
CoLA	47.40±7.97	56.08±0.15	70.26±0.39	52.36±2.02	51.80±0.15	OOM	10.8
HCM-A	43.99±0.72	52.38±0.64	41.69±1.75	51.35±0.85	54.84±1.56	OOM	13.0
TAM	56.06±2.19	58.35±1.91	69.95±2.00	50.51±0.14	OOM	OOM	9.0
Unsupervised - Pre-Train & Fine-Tune							
DOMINANT	59.06±2.80	60.60±0.11	73.63±0.16	47.44±0.64	OOM	OOM	7.3
CoLA	52.51±6.66	64.21±0.43	79.27±1.26	55.38±3.43	23.81±1.36	OOM	7.2
HCM-A	42.20±0.55	52.86±1.38	45.25±3.86	49.59±3.67	OOM	OOM	12.8
TAM	57.13±1.59	57.28±2.73	69.96±2.01	50.81±0.03	OOM	OOM	7.2
Generalist							
UNPrompt*	61.62±5.07	70.29±0.87	73.87±1.47	45.17±1.54	20.47±2.26	52.83±1.46	6.5
AnomalyGFM*	83.16±0.77	52.17±0.98	44.54±2.77	54.73±3.92	65.46±2.35	40.93±5.69	9.8
ARC (ours)	80.67±1.81	75.86±0.71	82.29±0.59	53.08±1.93	73.88±3.43	79.33±0.49	2.3
ARC _{zero} (ours)	83.76±1.01	75.30±0.92	82.67±0.10	51.70±0.86	75.47±0.31	78.84±0.12	2.4

applications. In contrast, the baseline methods under the “pre-train only” setting exhibit generally mediocre performance. Even when fine-tuning is applied – at the cost of additional computational resources and manual effort – these baselines often fail to match the performance of our methods.

- **Strong out-of-domain generalization ability.** The proposed methods, ARC and ARC_{zero}, demonstrate excellent performance on five out-of-domain datasets, even when the training datasets come from entirely different domains. This highlights their ability to adapt to new and unseen domains without requiring domain-specific fine-tuning. Such robust

cross-domain generalization is particularly valuable in real-world scenarios, where training data often differ significantly from the target application domains.

- **Zero-shot detection capability of ARC_{zero}.** Surprisingly, ARC_{zero} achieves competitive performance, even without using any labeled data during inference. In some scenarios, ARC_{zero} even outperforms ARC. This is because its iterative pseudo-context refinement progressively selects highly representative normal nodes to improve context quality over potentially noisy fixed few-shot examples, thereby enabling reliable zero-shot anomaly detection on unseen datasets.

TABLE III
PERFORMANCE OF ARC AND ITS VARIANTS IN TERMS OF AUROC.

Variant	Cora	CiteSeer	ACM	BlogCatalog	Facebook	Weibo	Reddit	Amazon
ARC	87.45±0.74	90.95±0.59	79.88±0.28	74.76±0.06	67.56±1.60	88.85±0.14	60.04±0.69	80.67±1.81
w/o A	80.65±0.71	83.35±0.64	79.29±0.16	73.86±0.18	62.80±2.06	89.69±0.17	54.60±1.92	64.76±2.13
w/o R	37.44±1.40	31.52±0.71	61.83±1.16	49.30±2.06	20.38±9.63	97.72±0.59	52.94±0.96	50.15±0.24
w/o C	47.39±0.42	53.98±0.72	54.24±1.32	60.46±1.23	48.86±0.97	42.84±3.01	51.03±0.86	69.02±0.97

TABLE IV
PERFORMANCE OF ARC_{zero} AND ITS VARIANTS IN TERMS OF AUROC.

Variant	Cora	CiteSeer	ACM	BlogCatalog	Facebook	Weibo	Reddit	Amazon
ARC _{zero}	87.54±0.57	91.20±0.27	78.78±0.17	74.75±0.03	69.25±0.95	88.71±0.18	59.57±0.42	83.76±1.01
w/o Iter. Score	87.76±0.60	90.13±0.39	79.23±0.13	74.71±0.15	67.78±1.00	88.17±0.13	59.13±0.53	80.85±1.64
w/o Multi-Round	87.37±0.55	91.48±0.26	79.70±0.09	74.47±0.04	65.52±0.93	88.25±0.13	58.16±0.74	80.92±1.09
w Random Init	86.47±0.17	90.10±0.21	79.69±0.04	74.15±0.13	65.40±1.12	79.36±4.32	58.92±0.33	82.91±0.27
w Degree Init	87.30±0.52	91.31±0.23	79.56±0.09	73.92±0.17	68.46±1.62	84.28±2.18	59.21±0.32	78.82±2.53
w Rep. Clu. Init	87.87±0.53	91.45±0.23	74.51±0.95	69.59±1.18	68.39±1.09	60.42±13.45	52.57±1.31	72.26±1.70

- **Scalability to large datasets.** Both ARC and ARC_{zero} exhibit strong scalability, performing effectively on large datasets such as T-Finance and Elliptic. This scalability is further demonstrated by their consistent performance even under resource constraints, such as when some baseline methods run out of memory (OOM).

C. Ablation Studies

To verify the effectiveness of key components and designs in ARC and ARC_{zero}, we conduct ablation studies by removing or modifying specific modules and evaluating their impact on performance. For brevity, we present only the results in terms of AUROC in ablation studies.

1) *Ablation Study for ARC:* To investigate the contributions of the three core components in ARC, we replace each component with an alternative design and construct three variants: 1) **w/o A:** using random projection to replace smoothness-based feature alignment module; 2) **w/o R:** using GCN to replace ego-neighbor residual graph encoder; and 3) **w/o C:** using binary classification-based predictor trained by binary cross-entropy loss to replace cross-attentive in-context anomaly scoring module. The results of the performance comparison are shown in Table III. From the table, we can see that all three components significantly contribute to the performance, as removing or replacing any of them leads to a notable drop in GAD performance. Among these components, the in-context anomaly scoring module proves to be crucial, as removing it (**w/o C**) results in performance that is nearly equivalent to random guessing on the majority of datasets. The residual graph encoder also plays a significant role, as we observe that removing this component leads to the performance flip issue [66] on certain datasets, indicating unreliable anomaly detection judgments. Notably, the Weibo dataset stands out as an exception, where the GCN encoder outperforms the residual graph encoder. This could be attributed to the unique anomaly patterns present in the Weibo dataset, which differ from those in the other datasets.

2) *Ablation Study for ARC_{zero}:* For ARC, we create two variants to discuss the impact of the key designs: 1) **w/o**

Iter. Score: using single step scoring based on initialized pseudo-normal nodes to replace iterative scoring and 2) **w/o Multi-Round:** using the predictions at the final iteration as the output anomaly scores. Meanwhile, to investigate the effectiveness of different initialization strategies, here we try three alternative ways, including random selection, mean-degree nodes as initialization, and clustering based on representations. The comparison results are demonstrated in Table IV, leading to the following observations. 1) Both iterative scoring and multi-round refinement prove to be critical components of ARC_{zero}. Removing iterative scoring results in consistently lower performance across datasets, highlighting the importance of iteratively refining the anomaly scores. Similarly, removing the multi-round process also degrades performance, particularly on datasets like Facebook and Reddit, where the iterative process aids in capturing complex patterns. 2) Among the initialization strategies, random selection shows the weakest performance, indicating that initialization with meaningful prior knowledge is essential. Using degree-based initialization slightly improves performance over random selection, as it exploits structural information about the graph. However, the representation-based clustering as initialization sometimes yields stronger results across most datasets. 3) Despite some variance in performance depending on the dataset, the full ARC_{zero} method outperforms all variants in most cases, showcasing the robustness and effectiveness of its design choices. These results further validate the necessity of incorporating both iterative scoring and multi-round refinement, as well as using an feature clustering-based initialization strategy.

D. Parameter Studies

In this subsection, we analyze the impact of the number of context nodes (i.e., n_k) on the performance of ARC and ARC_{zero}, respectively. For brevity, we present the results on four representative in-domain datasets.

1) *Effect of Few-Shot Sample Number in ARC:* Firstly, we vary the number of few-shot normal nodes (n_k in ARC) within the range of 2 to 100 to evaluate the few-shot efficiency of ARC. The results in terms of AUROC and AUPRC are illustrated

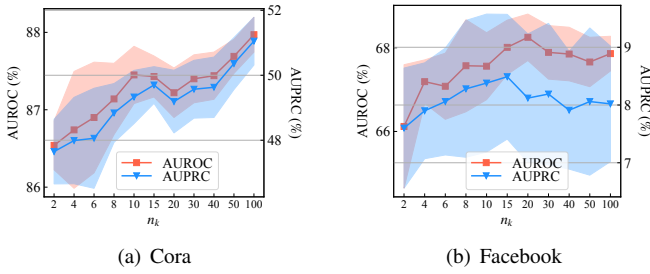


Fig. 5. Performance with varying n_k in few-shot method ARC. The shaded areas represent the standard deviation over 5 repeated runs.

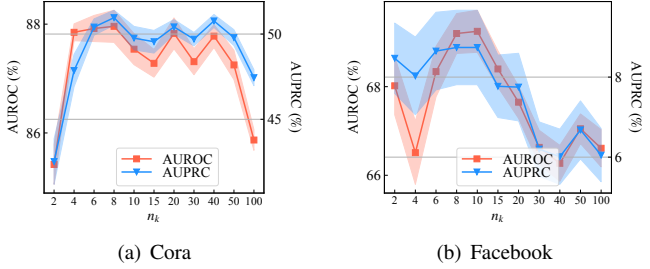


Fig. 6. Performance with varying n_k in zero-shot method ARC_{zero} . The shaded areas represent the standard deviation over 5 repeated runs.

in Fig. 5 (more results in Appendix D). From the figure, we observe that ARC consistently improves its performance as the number of few-shot normal nodes increases. Even with as few as $n_k = 6$ normal nodes, ARC achieves competitive performance on most datasets. This demonstrates the effectiveness of our approach in leveraging limited labeled information. Notably, the performance gain tends to plateau beyond $n_k = 50$ for many datasets, indicating that ARC efficiently utilizes the provided few-shot nodes without requiring a large number of labeled samples. This property makes ARC particularly suitable for scenarios where available labeled data is costly.

2) *Effect of Zero-Shot Pseudo-Normal Sample Number in ARC_{zero}* : Unlike in the few-shot counterpart, in our zero-shot method ARC_{zero} , n_k represents the number of pseudo-normal samples, making it a flexible hyperparameter that can influence the model’s performance. The experimental results in Fig. 6 (more results in Appendix D) reveal how varying n_k from 2 to 100 impacts the zero-shot GAD performance. From the plots, it is evident that the performance of ARC_{zero} is highly dependent on the choice of n_k . For some datasets (e.g. Cora), there is an optimal range of n_k (often between 6 and 50) where both AUROC and AUPRC reach their peak. Beyond this range, performance either plateaus or deteriorates, likely due to the inclusion of less informative and noisy (abnormal) pseudo-normal samples that may introduce noise. Other datasets, such as Facebook and Amazon, exhibit a more erratic trend, with performance fluctuating as n_k increases. This suggests that the quality and representativeness of pseudo-normal samples in these datasets are crucial, and a careful selection of n_k is required to balance model stability and performance.

E. Efficiency Analysis

In this experiment, we compare the running efficiency of the proposed methods and baselines. Specifically, we compare

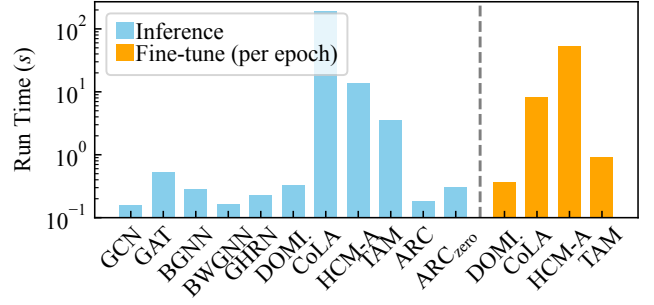


Fig. 7. Efficiency comparison of inference and fine-tuning time.

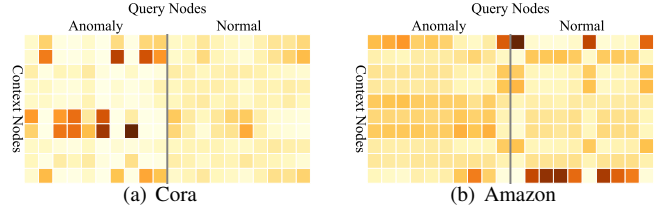


Fig. 8. Visualization of the attention weights of cross-attentive scoring module. Darker colors represent larger values.

the inference and fine-tuning times when applying the models to an unseen dataset, which is demonstrated in Fig. 7. The results demonstrate that ARC achieves a fast inference speed comparable to the most efficient baselines, highlighting its practicality for real-world applications. Additionally, the zero-shot version, ARC_{zero} , also exhibits relatively high efficiency, enabling zero-shot anomaly detection without the need for dataset-specific tuning. In contrast, dataset-specific fine-tuning imposes significant time costs. Even a single fine-tuning epoch for these baselines takes substantially longer than the inference phase of most methods, further underscoring the efficiency advantage of our generalist methods.

F. Visualization

1) *Visualization of Attention Weights*: To investigate the weight allocation mechanism of the cross-attentive in-context anomaly scoring module in ARC, we visualize the attention weights between context nodes and query nodes captured by the cross-attention block. The visualization results are illustrated in Fig. 8. In Fig. 8(a), we observe that ARC assigns relatively uniform attention weights to the normal nodes, leading to embeddings that closely mirror the average embedding of the surrounding context nodes. This indicates a more centralized representation of normal nodes. In contrast, anomalies are reconstructed using a selective combination of one or two context nodes, which results in embeddings that are more distanced from the central cluster. This behavior reflects the situation described in the “single-class normal” case in Fig. 4(a). On the other hand, Fig. 8(b) shows that each normal query node is allocated to multiple context nodes according to two distinct patterns, which is indicative of the “multi-class normal” scenario presented in Fig. 4(b). This highlights the versatility of ARC’s cross-attention module, which facilitates adaptation to different anomaly and normal node distribution patterns.

2) *Visualization of Representations*: To investigate the representation learning ability of our ego-neighbor residual

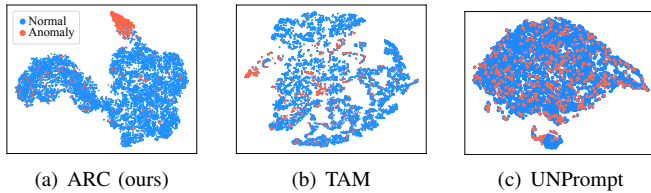


Fig. 9. t-SNE visualization of representations by ARC and baselines.

graph encoder, we visualize the representation distribution of Amazon, one of the testing datasets, learned by ARC and three baselines (TAM and UNPrompt) using t-SNE [67]. The visualizations in Fig. 9 demonstrate the effectiveness of our encoder in generating discriminative representations for normal and anomalous nodes compared to the baseline. Specifically, we can observe that the anomalous samples are mainly clustered into one or more small groups, which enhances the separability between normal and anomalous nodes. This phenomenon suggests that the encoder is able to effectively capture the underlying patterns of anomalies, making them more distinguishable from the normal nodes. Notably, these visualizations are based on the representations of the test data, which were never seen during the training phase. This showcases the generalization capability of the model, as it successfully adapts to unseen data and effectively captures underlying patterns in the node distributions.

VII. CONCLUSION AND OUTLOOK

While graph anomaly detection (GAD) has gained increasing research attention in recent years, the challenge of developing a universal and general GAD model that can be directly applied to any new dataset on-the-fly remains unresolved. This paper addresses this challenge by introducing the novel research problem of generalist GAD, which aims to develop models capable of detecting anomalies across diverse datasets without requiring task-specific fine-tuning. Firstly, we develop a few-shot generalist GAD method, termed ARC, which leverages in-context learning to effectively detect anomalies on an unseen dataset using only a few labeled normal samples. Building on ARC, we further propose a zero-shot variant, ARC_{zero} , which eliminates the need for labeled samples by generating pseudo-normal nodes for anomaly detection, enabling fully label-free generalization to unseen datasets. Extensive experiments conducted on diverse benchmark datasets demonstrate the effectiveness and efficiency of both ARC and ARC_{zero} , highlighting their ability to achieve competitive GAD performance across various domains and scenarios.

Limitations. Despite its promising performance, our study has some limitations that open avenues for future research. **Limitation 1:** In certain scenarios, ARC may be outperformed by ARC_{zero} . A possible explanation is that ARC_{zero} applies a filtering mechanism to context samples, which enhances the quality of the pseudo-normal nodes. **Limitation 2:** In ARC_{zero} , determining the optimal number of pseudo-normal nodes and ensuring that the selected nodes align well with the underlying data distribution remain open challenges. If the initial selection is not ideal, there is a risk of confirmation bias being amplified

during iterations, which could affect the model’s stability and generalization on unseen datasets. **Limitation 3:** From a theoretical perspective, providing formal guarantees for the proposed generalist GAD framework remains an open problem. **Future Directions.** In future research, several promising directions can be explored. 1) To handle **Limitation 1**, potential solutions include developing semi-supervised in-context learning frameworks that leverage both labeled and unlabeled samples or employing active learning strategies [68] that allow the model to select the most informative nodes to label. 2) To deal with **Limitation 2**, adaptive mechanisms can be developed to dynamically optimize the definition and selection of pseudo-normal nodes. For instance, one could add lightweight consistency or diversity constraints during pseudo-context selection (e.g., filtering nodes by cross-run stability) to further mitigate the impact of imperfect initialization and ensure robustness across varying data distributions. 3) While this work introduces the concept of generalist GAD, our focus is limited to node-level anomaly detection. Extending this concept to edge-level and graph-level GAD, or designing a universal model capable of accommodating anomalies at multiple scales, represents an exciting and promising direction for future exploration. 4) Although we focus on universal generalization without adaptation, investigating target-specific fine-tuning remains an interesting avenue to further probe the robustness of the learned parameter space.

ACKNOWLEDGMENT

The work of S. Pan was partially supported by ARC Grant No. DP240101547. The work of Y. Liu was partially supported by the ARC Grant No. DE260101172.

REFERENCES

- [1] K. Ding, J. Li, R. Bhanushali, and H. Liu, “Deep anomaly detection on attributed networks,” in *Proceedings of the 2019 SIAM International Conference on Data Mining*. SIAM, 2019, pp. 594–602.
- [2] Y. Liu, Z. Li, S. Pan, C. Gong, C. Zhou, and G. Karypis, “Anomaly detection on attributed networks via contrastive self-supervised learning,” *IEEE transactions on neural networks and learning systems*, vol. 33, no. 6, pp. 2378–2392, 2021.
- [3] J. Tang, J. Li, Z. Gao, and J. Li, “Rethinking graph neural networks for anomaly detection,” in *International Conference on Machine Learning*. PMLR, 2022, pp. 21 076–21 089.
- [4] H. Qiao, H. Tong, B. An, I. King, C. Aggarwal, and G. Pang, “Deep graph anomaly detection: A survey and new perspectives,” *arXiv preprint arXiv:2409.09957*, 2024.
- [5] X. Ma, J. Wu, S. Xue, J. Yang, C. Zhou, Q. Z. Sheng, H. Xiong, and L. Akoglu, “A comprehensive survey on graph anomaly detection with deep learning,” *IEEE Transactions on Knowledge and Data Engineering*, vol. 35, no. 12, pp. 12 012–12 038, 2021.
- [6] R. Miao, Y. Liu, Y. Wang, X. Shen, Y. Tan, Y. Dai, S. Pan, and X. Wang, “Blindguard: Safeguarding llm-based multi-agent systems under unknown attacks,” *arXiv preprint arXiv:2508.08127*, 2025.
- [7] Y. Dou, Z. Liu, L. Sun, Y. Deng, H. Peng, and P. S. Yu, “Enhancing graph neural network-based fraud detectors against camouflaged fraudsters,” in *Proceedings of the 29th ACM international conference on information & knowledge management*, 2020, pp. 315–324.
- [8] C. Wang and H. Zhu, “Wrongdoing monitor: A graph-based behavioral anomaly detection in cyber security,” *IEEE Transactions on Information Forensics and Security*, vol. 17, pp. 2703–2718, 2022.
- [9] Y. Wu, H.-N. Dai, and H. Tang, “Graph neural networks for anomaly detection in industrial internet of things,” *IEEE Internet of Things Journal*, vol. 9, no. 12, pp. 9214–9231, 2021.
- [10] H. Qiao and G. Pang, “Truncated affinity maximization: One-class homophily modeling for graph anomaly detection,” in *Advances in Neural Information Processing Systems*, vol. 36, 2023.

- [11] Y. Gao, X. Wang, X. He, Z. Liu, H. Feng, and Y. Zhang, "Addressing heterophily in graph anomaly detection: A perspective of graph spectrum," in *Proceedings of the ACM Web Conference 2023*, 2023, pp. 1528–1538.
- [12] J. Tang, F. Hua, Z. Gao, P. Zhao, and J. Li, "Gadbench: Revisiting and benchmarking supervised graph anomaly detection," *Advances in Neural Information Processing Systems*, vol. 36, 2024.
- [13] Y. Zhao, Y. Liu, S. Li, Q. Chen, Y. Zheng, and S. Pan, "Freegad: A training-free yet effective approach for graph anomaly detection," in *Proceedings of the 34th ACM International Conference on Information and Knowledge Management*, 2025, pp. 4379–4389.
- [14] J. Pan, Y. Zheng, Y. Tan, and Y. Liu, "A survey of generalization of graph anomaly detection: From transfer learning to foundation models," in *The 16th IEEE International Conference on Knowledge Graphs*, 2025.
- [15] J. Pan, Y. Liu, C. Zhou, F. Xiong, A. W.-C. Liew, and S. Pan, "Correcting false alarms from unseen: Adapting graph anomaly detectors at test time," in *Proceedings of the AAAI Conference on Artificial Intelligence*, 2026.
- [16] J. Zhu and G. Pang, "Toward generalist anomaly detection via in-context residual learning with few-shot sample prompts," in *Proceedings of the IEEE/CVF Conference on Computer Vision and Pattern Recognition*, 2024.
- [17] K. Dong, H. Mao, Z. Guo, and N. V. Chawla, "Universal link predictor by in-context learning," *arXiv preprint arXiv:2402.07738*, 2024.
- [18] C. Niu, H. Qiao, C. Chen, L. Chen, and G. Pang, "Zero-shot generalist graph anomaly detection with unified neighborhood prompts," in *Proceedings of the International Joint Conference on Artificial Intelligence*, 2025.
- [19] H. Zhao, A. Chen, X. Sun, H. Cheng, and J. Li, "All in one and one for all: A simple yet effective method towards cross-domain graph pretraining," in *Proceedings of the 30th ACM SIGKDD Conference on Knowledge Discovery and Data Mining*, 2024, pp. 4443–4454.
- [20] Y. Liu, S. Li, Y. Zheng, Q. Chen, C. Zhang, and S. Pan, "Arc: A generalist graph anomaly detector with in-context learning," in *Advances in Neural Information Processing Systems*, 2024.
- [21] I. Ahmed, T. Galoppo, X. Hu, and Y. Ding, "Graph regularized autoencoder and its application in unsupervised anomaly detection," *IEEE transactions on pattern analysis and machine intelligence*, vol. 44, no. 8, pp. 4110–4124, 2021.
- [22] L. Ruff, R. Vandermeulen, N. Goernitz, L. Deecke, S. A. Siddiqui, A. Binder, E. Müller, and M. Kloft, "Deep one-class classification," in *International conference on machine learning*. PMLR, 2018, pp. 4393–4402.
- [23] T. Xiang, Y. Zhang, Y. Lu, A. Yuille, C. Zhang, W. Cai, and Z. Zhou, "Exploiting structural consistency of chest anatomy for unsupervised anomaly detection in radiography images," *IEEE Transactions on Pattern Analysis and Machine Intelligence*, 2024.
- [24] C. Zhou and R. C. Paffenroth, "Anomaly detection with robust deep autoencoders," in *Proceedings of the 23rd ACM SIGKDD international conference on knowledge discovery and data mining*, 2017, pp. 665–674.
- [25] K. Roth, L. Pemula, J. Zepeda, B. Schölkopf, T. Brox, and P. Gehler, "Towards total recall in industrial anomaly detection," in *Proceedings of the IEEE/CVF Conference on Computer Vision and Pattern Recognition*, 2022, pp. 14 318–14 328.
- [26] T. Defard, A. Setkov, A. Loesch, and R. Audigier, "Padim: a patch distribution modeling framework for anomaly detection and localization," in *International Conference on Pattern Recognition*. Springer, 2021, pp. 475–489.
- [27] V. Schwag, M. Chiang, and P. Mittal, "SSD: A unified framework for self-supervised outlier detection," in *International Conference on Learning Representations*, 2021.
- [28] J. Jeong, Y. Zou, T. Kim, D. Zhang, A. Ravichandran, and O. Dabeer, "Winclip: Zero-/few-shot anomaly classification and segmentation," in *Proceedings of the IEEE/CVF Conference on Computer Vision and Pattern Recognition*, 2023, pp. 19 606–19 616.
- [29] J. Su, C. Jiang, X. Jin, Y. Qiao, T. Xiao, H. Ma, R. Wei, Z. Jing, J. Xu, and J. Lin, "Large language models for forecasting and anomaly detection: A systematic literature review," *arXiv preprint arXiv:2402.10350*, 2024.
- [30] Q. Zhou, G. Pang, Y. Tian, S. He, and J. Chen, "Anomalyclip: Object-agnostic prompt learning for zero-shot anomaly detection," in *International Conference on Learning Representations*, 2024.
- [31] J. Li, H. Dani, X. Hu, and H. Liu, "Radar: Residual analysis for anomaly detection in attributed networks," in *IJCAI*, vol. 17, 2017, pp. 2152–2158.
- [32] Z. Peng, M. Luo, J. Li, H. Liu, Q. Zheng *et al.*, "Anomalous: A joint modeling approach for anomaly detection on attributed networks," in *IJCAI*, vol. 18, 2018, pp. 3513–3519.
- [33] M. He, Z. Wei, H. Xu *et al.*, "Bernnet: Learning arbitrary graph spectral filters via bernstein approximation," *Advances in Neural Information Processing Systems*, vol. 34, pp. 14 239–14 251, 2021.
- [34] H. Fan, F. Zhang, and Z. Li, "Anomalydae: Dual autoencoder for anomaly detection on attributed networks," in *ICASSP 2020-2020 IEEE International Conference on Acoustics, Speech and Signal Processing (ICASSP)*. IEEE, 2020, pp. 5685–5689.
- [35] T. Huang, Y. Pei, V. Menkovski, and M. Pechenizkiy, "Hop-count based self-supervised anomaly detection on attributed networks," in *Joint European conference on machine learning and knowledge discovery in databases*. Springer, 2022, pp. 225–241.
- [36] J. Pan, Y. Liu, Y. Zheng, and S. Pan, "Prem: A simple yet effective approach for node-level graph anomaly detection," in *2023 IEEE International Conference on Data Mining (ICDM)*. IEEE, 2023, pp. 1253–1258.
- [37] K. Ding, K. Shu, X. Shan, J. Li, and H. Liu, "Cross-domain graph anomaly detection," *IEEE Transactions on Neural Networks and Learning Systems*, vol. 33, no. 6, pp. 2406–2415, 2021.
- [38] Q. Wang, G. Pang, M. Salehi, W. Buntine, and C. Leckie, "Cross-domain graph anomaly detection via anomaly-aware contrastive alignment," in *Proceedings of the AAAI Conference on Artificial Intelligence*, vol. 37, 2023, pp. 4676–4684.
- [39] H. Qiao, C. Niu, L. Chen, and G. Pang, "Anomalygfm: Graph foundation model for zero/few-shot anomaly detection," in *Proceedings of the 31st ACM SIGKDD Conference on Knowledge Discovery and Data Mining V. 2*, 2025, pp. 2326–2337.
- [40] Q. Dong, L. Li, D. Dai, C. Zheng, J. Ma, R. Li, H. Xia, J. Xu, Z. Wu, B. Chang *et al.*, "A survey on in-context learning," in *Proceedings of the 2024 Conference on Empirical Methods in Natural Language Processing*, 2024, pp. 1107–1128.
- [41] J.-B. Alayrac, J. Donahue, P. Luc, A. Miech, I. Barr, Y. Hasson, K. Lenc, A. Mensch, K. Millican, M. Reynolds *et al.*, "Flamingo: a visual language model for few-shot learning," *Advances in neural information processing systems*, vol. 35, pp. 23 716–23 736, 2022.
- [42] A. Bar, Y. Gandelsman, T. Darrell, A. Globerson, and A. Efros, "Visual prompting via image inpainting," *Advances in Neural Information Processing Systems*, vol. 35, pp. 25 005–25 017, 2022.
- [43] Q. Huang, H. Ren, P. Chen, G. Kržmanc, D. Zeng, P. S. Liang, and J. Leskovec, "Prodigy: Enabling in-context learning over graphs," *Advances in Neural Information Processing Systems*, vol. 36, 2024.
- [44] H. Abdi and L. J. Williams, "Principal component analysis," *Wiley interdisciplinary reviews: computational statistics*, vol. 2, no. 4, pp. 433–459, 2010.
- [45] H. Liu, J. Feng, L. Kong, N. Liang, D. Tao, Y. Chen, and M. Zhang, "One for all: Towards training one graph model for all classification tasks," in *International Conference on Learning Representations*, 2024.
- [46] Y. Dong, K. Ding, B. Jalaian, S. Ji, and J. Li, "Adagmn: Graph neural networks with adaptive frequency response filter," in *Proceedings of the 30th ACM international conference on information & knowledge management*, 2021, pp. 392–401.
- [47] X. Zheng, Y. Wang, Y. Liu, M. Li, M. Zhang, D. Jin, P. S. Yu, and S. Pan, "Graph neural networks for graphs with heterophily: A survey," *arXiv preprint arXiv:2202.07082*, 2022.
- [48] T. N. Kipf and M. Welling, "Semi-supervised classification with graph convolutional networks," in *International Conference on Learning Representations*, 2017.
- [49] P. Veličković, G. Cucurull, A. Casanova, A. Romero, P. Lio, and Y. Bengio, "Graph attention networks," in *International Conference on Learning Representations*, 2018.
- [50] F. Wu, A. Souza, T. Zhang, C. Fifty, T. Yu, and K. Weinberger, "Simplifying graph convolutional networks," in *International conference on machine learning*. PMLR, 2019, pp. 6861–6871.
- [51] H. Bahonar, A. Mirzaei, S. Sadri, and R. C. Wilson, "Graph embedding using frequency filtering," *IEEE transactions on pattern analysis and machine intelligence*, vol. 43, no. 2, pp. 473–484, 2019.
- [52] A. Vaswani, N. Shazeer, N. Parmar, J. Uszkoreit, L. Jones, A. N. Gomez, Ł. Kaiser, and I. Polosukhin, "Attention is all you need," *Advances in neural information processing systems*, vol. 30, 2017.
- [53] R. Rombach, A. Blattmann, D. Lorenz, P. Esser, and B. Ommer, "High-resolution image synthesis with latent diffusion models," in *Proceedings of the IEEE/CVF conference on computer vision and pattern recognition*, 2022, pp. 10 684–10 695.
- [54] J. A. Hartigan, M. A. Wong *et al.*, "A k-means clustering algorithm," *Applied statistics*, vol. 28, no. 1, pp. 100–108, 1979.
- [55] O. Shchur, M. Mumme, A. Bojchevski, and S. Günnemann, "Pitfalls of graph neural network evaluation," in *NeurIPS Workshop*, 2018.
- [56] P. Sen, G. Namata, M. Bilgic, L. Getoor, B. Galligher, and T. Eliassi-Rad, "Collective classification in network data," *AI magazine*, vol. 29, no. 3, pp. 93–93, 2008.

- [57] J. Tang, J. Zhang, L. Yao, J. Li, L. Zhang, and Z. Su, "Arnetminer: extraction and mining of academic social networks," in *Proceedings of the 14th ACM SIGKDD international conference on Knowledge discovery and data mining*, 2008, pp. 990–998.
- [58] L. Tang and H. Liu, "Relational learning via latent social dimensions," in *Proceedings of the 15th ACM SIGKDD international conference on Knowledge discovery and data mining*, 2009, pp. 817–826.
- [59] Z. Xu, X. Huang, Y. Zhao, Y. Dong, and J. Li, "Contrastive attributed network anomaly detection with data augmentation," in *Pacific-Asia Conference on Knowledge Discovery and Data Mining*. Springer, 2022, pp. 444–457.
- [60] S. Kumar, X. Zhang, and J. Leskovec, "Predicting dynamic embedding trajectory in temporal interaction networks," in *Proceedings of the 25th ACM SIGKDD international conference on knowledge discovery & data mining*, 2019, pp. 1269–1278.
- [61] O. Platonov, D. Kuznedelev, M. Diskin, A. Babenko, and L. Prokhorenkova, "A critical look at the evaluation of gnns under heterophily: Are we really making progress?" in *Proceedings of the Twelfth International Conference on Learning Representations*, 2023.
- [62] S. Rayana and L. Akoglu, "Collective opinion spam detection: Bridging review networks and metadata," in *Proceedings of the 21th acm sigkdd international conference on knowledge discovery and data mining*, 2015, pp. 985–994.
- [63] J. J. McAuley and J. Leskovec, "From amateurs to connoisseurs: modeling the evolution of user expertise through online reviews," in *Proceedings of the 22nd international conference on World Wide Web*, 2013, pp. 897–908.
- [64] M. Weber, G. Domeniconi, J. Chen, D. K. I. Weidele, C. Bellei, T. Robinson, and C. E. Leiserson, "Anti-money laundering in bitcoin: Experimenting with graph convolutional networks for financial forensics," in *KDD Workshop*, 2019.
- [65] S. Ivanov and L. Prokhorenkova, "Boost then convolve: Gradient boosting meets graph neural networks," in *International Conference on Learning Representations*, 2021.
- [66] L. Zhao and L. Akoglu, "On using classification datasets to evaluate graph outlier detection: Peculiar observations and new insights," *Big Data*, vol. 11, no. 3, pp. 151–180, 2023.
- [67] L. Van der Maaten and G. Hinton, "Visualizing data using t-sne." *Journal of machine learning research*, vol. 9, no. 11, 2008.
- [68] Z. Chen, J. Duan, L. Kang, and G. Qiu, "Supervised anomaly detection via conditional generative adversarial network and ensemble active learning," *IEEE Transactions on Pattern Analysis and Machine Intelligence*, vol. 45, no. 6, pp. 7781–7798, 2022.

APPENDIX A
 ADDITIONAL EXPLANATIONS FOR DATASETS WITH
 ATYPICAL RESULTS

We provide additional explanations for the datasets used in our experiments, including their anomaly definitions and characteristics.

- **Cora, CiteSeer, PubMed [56], and ACM [57]** are citation networks, where nodes are publications and edges denote citation links. Node attributes are bag-of-words features.
- **BlogCatalog and Flickr [1], [58]** are social networks with injected anomalies, where nodes are users and edges represent following relationships. Node attributes are derived from user-generated textual content (e.g., posts, tags).
- **Amazon and YelpChi [62], [63]** are review-related graphs with real anomalies. In this work, we use Amazon-UPU and YelpChi-RUR, following the standard constructions based on user and review relations [10].
- **Facebook [59]** is a social network with real anomalies, where nodes are users and edges represent friendship relationships.
- **Reddit [60]** is a forum interaction network, where banned users are treated as anomalies. Node attributes are derived from textual content.
- **Weibo [60]** is a microblog user-hashtag graph, where users with frequent suspicious posting behaviors in a short time window are labeled as anomalies. Node features include location and bag-of-words features.
- **Questions [61]** is a Q&A interaction network from Yandex Q, where nodes are users and edges indicate question-answer interactions. Node features are based on FastText embeddings of user descriptions.
- **Tolokers [61]** is a crowd-sourcing worker graph from the Toloka platform, where nodes are workers and edges connect workers who have worked on the same task. The task is to identify banned workers, and node features are based on worker profiles and task performance statistics.
- **T-Finance [3]** is a transaction network, where nodes are anonymized accounts with 10-dimensional features (e.g., registration days, login activities, and interaction frequency) and edges indicate transaction records between accounts. Anomalies are accounts annotated by experts (e.g., fraud, money laundering, and online gambling).
- **Elliptic [64]** is a Bitcoin transaction graph with directed payment flows, where nodes are transactions and edges denote payments. The nodes are associated with licit entities (e.g., exchanges and wallet providers) or illicit categories (e.g., scams, malware, ransomware, and Ponzi schemes), and anomalies correspond to illicit transactions.

Anomaly Injection. For datasets with injected anomalies, we follow the common protocol in [1], [2] to inject both structural and attribute anomalies.

APPENDIX B
 COMPLEXITY ANALYSIS

We summarize the time complexity of the overall inference pipeline (including ARC_{zero} in Alg. 1) by decomposing it into

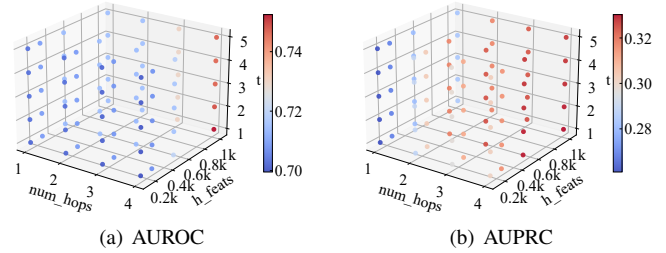


Fig. 10. Hyperparameter sensitivity analysis.

feature alignment, embedding generation, and anomaly scoring.

In the testing phase, the time complexity consists of two main components: feature alignment and model inference. For feature alignment, the overall complexity is $\mathcal{O}(n d d_u + d_u m + d_u \log(d_u))$, where $m = |\mathcal{E}|$ is the number of edges. Here, the first term is used for feature projection, while the second and third terms are used for smoothness computation and feature reordering, respectively. The model inference is divided into two main parts: embedding generation and anomaly scoring. The complexity of node embedding generation is $\mathcal{O}(L(m d_u + n d_u h + n h^2))$, where the first term is used for feature propagation and the rest of the terms are used for residual encoding by MLP. The anomaly scoring, on the other hand, mainly involves cross-attention computation with time complexity of $\mathcal{O}(n_q n_k h + n_q h)$, where n_q is the number of query nodes and n_k is the number of context nodes.

For ARC_{zero}, the additional computational costs primarily stem from pseudo-context initialization and iterative pseudo-context refinement. The initialization employs K-means clustering on the aligned features, which has a time complexity of $\mathcal{O}(t_{km} n d_u n_k)$, where t_{km} is the number of clustering iterations. The iterative process repeats the anomaly scoring and context selection for T rounds. Consequently, the complexity of this phase is $\mathcal{O}(T(n_q n_k h + n_q h + n_q \log n_q))$, where the last term accounts for sorting the query nodes to update context. Since t_{km} and T are small constants, ARC_{zero} maintains a comparable efficiency to ARC.

APPENDIX C
 ALGORITHM

The algorithm pseudocode of ARC_{zero} is described in Algo 1.

APPENDIX D
 ADDITIONAL EXPERIMENTAL DETAILS

A. Hyperparameter Sensitivity Study

The hyperparameter sensitivity results in Fig. 10 indicate that the performance is relatively stable across a broad range of configurations. In general, increasing the representation dimension h_{feats} tends to improve both AUROC and AUPRC, while varying the propagation depth (`num_hops`) and the iteration steps t only introduces mild fluctuations. This suggests that our method does not rely on delicate hyperparameter tuning and remains robust under different settings.

Algorithm 1: The Inference Algorithm of ARC_{zero}

Input: Test dataset \mathcal{D} with graph $\mathcal{G} = (\mathcal{V}, \mathcal{E}, \mathbf{X})$.

Parameters: Well-trained model parameters;
propagation iteration L ; pseudo-context size n_k ; refinement rounds T .

- 1 Align features in \mathcal{G} via the smoothness-based feature alignment
 - 2 Obtain aligned graph $\mathcal{G} = (\mathcal{V}, \mathcal{E}, \mathbf{X}')$
 - 3 **for** $l = 1 : L$ **do**
 - 4 $\mathbf{Z}^{[l]} \leftarrow$ Propagate and transform $\mathbf{X}' = \mathbf{X}^{[0]}$ via Eq. (3)
 - 5 $\mathbf{R}^{[l]} \leftarrow$ Calculate residual of $\mathbf{Z}^{[l]}$ via Eq. (4)
 - 6 **end**
 - 7 $\mathbf{H} \leftarrow$ Concatenate $[\mathbf{R}^{[1]} || \dots || \mathbf{R}^{[L]}]$ via Eq. (4)
 - 8 Initialize pseudo-context nodes $\mathcal{V}_k^{[1]}$ by running k -means on aligned features \mathbf{X}' and selecting n_k pseudo-normal nodes
 - 9 **for** $t = 1 : T$ **do**
 - 10 Separate \mathcal{V} into $\mathcal{V}_k^{[t]}$ and $\mathcal{V}_q^{[t]} = \mathcal{V} \setminus \mathcal{V}_k^{[t]}$
 - 11 Obtain $\mathbf{H}_k^{[t]}$ and $\mathbf{H}_q^{[t]}$ by indexing \mathbf{H} with $\mathcal{V}_k^{[t]}$ and $\mathcal{V}_q^{[t]}$, respectively
 - 12 $\tilde{\mathbf{H}}_q^{[t]} \leftarrow$ Calculate cross attention from $\mathbf{H}_q^{[t]}$ and $\mathbf{H}_k^{[t]}$ via Eq. (6)
 - 13 Compute anomaly scores $f(v_i)^{[t]}$ for all $v_i \in \mathcal{V}_q^{[t]}$ by the distance between $\tilde{\mathbf{H}}_q^{[t]}$ and $\mathbf{H}_q^{[t]}$
 - 14 Impute scores of pseudo-context nodes by setting $f(v_i)^{[t]} \leftarrow \min_{v_j \in \mathcal{V}_q^{[t]}} \{f(v_j)^{[t]}\}$ for $v_i \in \mathcal{V}_k^{[t]}$
 - 15 Update pseudo-context nodes $\mathcal{V}_k^{[t+1]}$ by selecting the top- k (here $k = n_k$) nodes with the smallest scores from $\mathcal{V}_q^{[t]}$
 - 16 **end**
 - 17 Return the final anomaly score $f(v_i) = \frac{1}{T} \sum_{t=1}^T f(v_i)^{[t]}$ for each $v_i \in \mathcal{V}$
-

B. AUPRC Performance Comparison

Table V reports the AUPRC results and leads to conclusions consistent with the AUROC comparison in the main text. Overall, ARC and ARC_{zero} achieve the strongest AUPRC performance on most datasets and obtain top average ranks, demonstrating robust generalization under both few-shot and zero-shot settings. In particular, our methods outperform the latest generalist baselines (UNPrompt and AnomalyGFM) in overall AUPRC across the test suite.

C. Additional Shot-Number Analysis

These additional few-shot results are consistent with the main observations: increasing n_k generally improves performance and then saturates. In particular, CiteSeer shows a clearer monotonic gain with larger n_k , while Amazon exhibits a faster saturation and slightly larger fluctuations, suggesting that a moderate number of context nodes is sufficient in practice.

Compared with the few-shot case, the zero-shot curves are more sensitive to n_k , since pseudo-context quality depends on the selected pseudo-normal nodes. We observe that CiteSeer

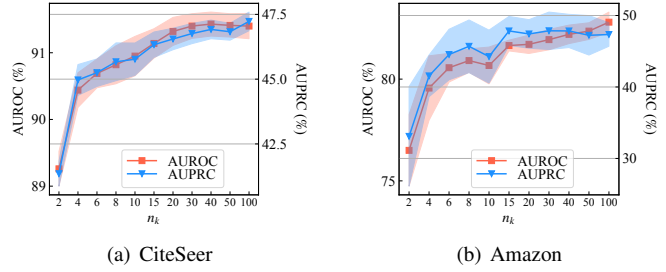


Fig. 11. Additional results for varying n_k in the few-shot setting (ARC).

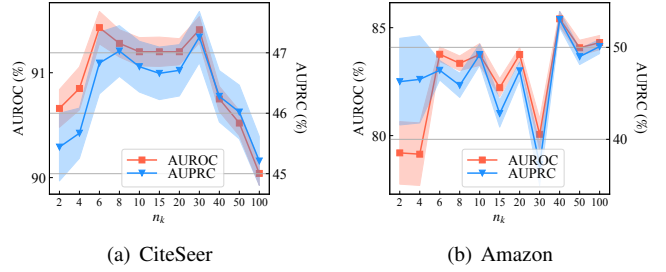


Fig. 12. Additional results for varying n_k in the zero-shot setting (ARC_{zero}).

achieves stable performance within a moderate range of n_k , while Amazon shows more noticeable fluctuations when n_k becomes large, indicating that overly large pseudo-context sets may introduce noisy nodes and reduce stability.

TABLE V

ANOMALY DETECTION PERFORMANCE IN TERMS OF AUPRC (IN PERCENT, MEAN±STD). HIGHLIGHTED ARE THE RESULTS RANKED **FIRST**, **SECOND**, AND **THIRD**. “RANK” INDICATES THE AVERAGE RANKING OVER 13 DATASETS. SUPERSCRIPIT “*” ON A BASELINE METHOD NAME INDICATES THAT OUR METHOD IS SIGNIFICANTLY DIFFERENT FROM THIS BASELINE ON ALL_DATASETS_TRIAL_AVG (PAIRED T-TEST AND WILCOXON TEST, P<0.05).

Method	Cora	CiteSeer	ACM	BlogCatalog	Facebook	Weibo	Reddit
Supervised - Pre-Train Only							
GCN	7.41±1.55	6.40±1.40	5.27±1.12	7.44±1.07	1.59±0.11	67.21±15.20	3.39±0.39
GAT	6.49±0.84	5.58±0.62	4.70±0.75	12.81±2.08	3.14±0.37	33.34±9.80	3.73±0.54
BGNN	4.90±1.27	3.91±1.01	3.48±1.33	5.73±1.47	3.81±2.12	30.26±29.98	3.52±0.50
BWGNN	7.25±0.80	6.35±0.73	7.14±0.20	8.99±1.12	2.54±0.63	12.13±0.71	3.69±0.81
GHRN	9.56±2.40	7.79±2.01	5.61±0.71	10.94±2.56	2.41±0.62	28.53±7.38	3.24±0.33
Unsupervised - Pre-Train Only							
DOMINANT	12.75±0.71	13.85±2.34	15.59±2.69	35.22±0.87	2.95±0.06	81.47±0.22	3.49±0.44
CoLA	11.41±3.51	8.33±3.73	7.31±1.45	6.04±0.56	1.90±0.68	7.59±3.26	3.71±0.67
HCM-A	5.78±0.76	4.18±0.75	4.01±0.61	6.89±0.34	2.08±0.60	21.91±11.78	3.18±0.23
TAM	11.18±0.75	11.55±0.44	23.20±2.36	10.57±1.17	8.40±0.97	16.46±0.09	3.94±0.13
Unsupervised - Pre-Train & Fine-Tune							
DOMINANT	21.35±0.74	23.02±1.55	22.74±0.95	35.79±0.63	3.56±0.15	77.69±1.43	3.84±0.74
CoLA	13.91±5.56	19.51±3.73	8.48±0.51	10.43±1.22	15.19±11.04	8.03±1.19	4.07±0.13
HCM-A	6.41±1.33	4.76±0.51	4.41±0.63	6.62±0.14	2.23±0.76	27.20±5.53	3.10±0.19
TAM	13.62±0.53	18.66±1.41	58.04±8.17	13.90±0.53	11.11±3.20	16.47±0.08	3.93±0.09
Generalist							
UNPrompt*	10.14±0.97	11.15±1.26	19.36±2.16	30.81±1.46	8.97±3.58	20.27±1.93	4.16±0.19
AnomalyGFM*	6.40±0.86	4.62±0.31	4.07±0.48	5.21±0.20	29.06±13.56	18.48±5.59	3.57±0.33
ARC (ours)	49.33±1.64	45.77±1.25	40.62±0.10	36.06±0.18	8.38±2.39	64.18±0.55	4.48±0.28
ARC _{zero} (ours)	49.76±1.37	46.77±0.84	40.12±0.15	35.26±0.31	8.74±1.86	64.27±0.41	4.34±0.08
Method	Amazon	Amazon-Photo	Coauthor-CS	Tolokers	T-Finance	Elliptic	Rank
Supervised - Pre-Train Only							
GCN	6.96±2.04	7.50±0.13	5.23±0.14	26.66±2.56	10.60±4.13	2.24±0.37	10.1
GAT	15.74±17.85	8.21±4.61	5.51±1.53	20.40±5.03	4.28±0.87	2.73±0.95	9.3
BGNN	7.51±0.58	7.34±0.59	5.06±0.15	22.25±4.30	6.35±2.27	2.14±0.17	12.1
BWGNN	13.12±11.82	7.55±1.40	5.59±1.84	20.10±3.62	11.67±8.02	2.34±0.29	10.0
GHRN	7.54±2.01	7.06±0.22	6.65±0.51	30.31±5.24	7.72±4.97	2.29±0.37	9.2
Unsupervised - Pre-Train Only							
DOMINANT	6.11±0.29	11.94±1.01	21.30±0.51	21.49±1.47	OOM	OOM	8.8
CoLA	11.06±4.45	6.74±0.28	9.46±0.32	23.97±2.01	5.04±0.75	OOM	10.8
HCM-A	5.87±0.07	5.90±0.10	2.63±0.09	22.64±0.17	7.19±0.94	OOM	14.0
TAM	10.75±3.10	8.56±1.90	17.99±2.94	22.84±0.06	OOM	OOM	8.7
Unsupervised - Pre-Train & Fine-Tune							
DOMINANT	7.48±0.46	22.18±0.29	23.30±0.22	20.38±1.99	OOM	OOM	7.2
CoLA	7.27±1.13	9.21±0.31	25.77±3.11	25.29±3.02	2.91±0.04	OOM	7.6
HCM-A	5.64±0.09	6.04±0.25	2.88±0.27	21.85±2.14	OOM	OOM	14.2
TAM	11.56±1.80	7.31±0.63	18.01±2.93	22.97±0.07	OOM	OOM	7.7
Generalist							
UNPrompt*	9.57±1.74	18.11±3.96	13.94±2.99	19.37±0.52	2.64±0.07	2.22±0.10	7.9
AnomalyGFM*	54.70±1.11	6.80±0.25	2.83±0.20	26.82±1.71	11.18±2.84	1.74±0.19	10.2
ARC (ours)	44.25±7.41	33.02±1.33	36.51±0.12	23.53±0.79	19.00±4.44	8.47±0.51	2.6
ARC _{zero} (ours)	49.21±2.29	29.69±5.70	36.34±0.35	23.05±0.32	24.52±0.70	8.42±0.1	2.7